frontiers

Transverse and quantum localization of light: a review on theory and experiments

Taira Giordani [1,3], **Walter Schirmacher** [2] **Giancarlo Ruocco** [1,3] **and Marco Leonetti** [3,4,*]

[1] *Department of Physics, University Sapienza, Roma, Italy*
[2] *Institut für Physik, Universität Mainz, Mainz, Germany* [3] *Center for Life Nano Science@Sapienza, Istituto Italiano di Tecnologia, Rome, Italia* [4] *CNR NANOTEC-Institute of Nanotechnology, Soft and Living Matter Lab, Rome, Italy*

Correspondence*:
Corresponding Author
marco.leonetti@nanotec.cnr.it

ABSTRACT

Anderson Localization is an interference effect yielding a drastic reduction of diffusion of wave packets such as sound, electromagnetic waves, and particle wave functions in the presence of strong disorder. In optics, this effect has been observed and demonstrated unquestionably only in dimensionally reduced systems. In particular, transverse localization (TL) occurs in optical fibers, which are disordered rectangular to, and translationally invariant along, the propagation direction. The resonant and tube-shaped localized states act as micro-fiber-like single-mode transmission channels. Since the proposal of the first TL models in the early eighties, the fabrication technology and experimental probing techniques, took giant steps forwards: TL has been observed in photorefractive crystals, in plastic optical fibers, and also in glassy platforms, while employing direct laser writing, it is now possible to tailor and “design” disorder. This review covers all these aspects that are today making TL closer to applications such as quantum communication or image transport. We first discuss nonlinear optical phenomena in the TL regime, enabling steering of optical communication channels. Then we report on experiments concerning the nature of the transversally localized states, showing a behavior of the localization strength with wavelength unexpected by the traditional theoretical model. We present a new consistent theoretical approach capable of describing all aspects of TL. Finally, we report on some quantum aspects, showing how a single-photon state can be localized in some of its inner degrees of freedom and how quantum phenomena can be employed to secure a quantum communication channel.

Keywords: Classical Optics, Photonics, Quantum Optics, Nonlinear Optics, Laser Writing

1 INTRODUCTION

Transverse localization (TL) is found in media in which the refractive index is randomly modulated only orthogonally to the direction of propagation. In these paraxial systems, AL sustains nondiffracting beams: confined light tubes showing many potential applications including, fiber optics, quantum communication, and endoscopic imaging. In this review we will review recent advances in disordered optical fibers, in which confinement is obtained thanks to localization, discussing the advantages with respect to standard fibers. First we will report about the latest experimental results on Transverse Anderson Localization: the

migration of localized states due to nonlinearity, self-focusing, wavefront shaping in the localized regime, and the single-mode transport in disordered paraxial structures. This last result is particularly important as it bridges the physics of Anderson Localization to the single-mode properties of optical fibers.

Then we will show how the traditional description of Anderson localization, which was based on the analogy to electrons in a random potential, turned out to be in error and led to the prediction of a localization length depending strongly on the wavelength of the light, which was not observed. We also report on the alternative correct theory, which relies on an analogy to acoustical waves in the presence of random elastic moduli. Regarding quantum aspects, we will report on how a single-photon state localized in some of its inner degrees of freedom could be an effective resource in quantum communication and cryptography, increasing both the amount of information loaded per single particle and the security and performance of protocols based on localized photon quanta. Finally, we will review the so-called random quantum walks in which the dynamics of a single particle moving on a lattice conditionally to the state of an ancillary degree of freedom, display localization under certain conditions. A further aspect of AL of quantum particles is the behavior of the multi-particle interference and of the particle statistics in quantum walks. In the first proof-of-principle photonic experiments AL has been observed in the two-photon wavefunction. In this scenario, it could be possible to simulate even the fermionic statistics by proper manipulation of two-photon entangled states generated by single-photon sources.

1.1 Modeling transverse localization: the beginning

In the last decades, the idea that Anderson localization could be applied to electromagnetic waves[1, 2] has drawn the attention of the scientific community, stimulating experiments and conjectures. The excitement was further propelled by the following observation of the coherent backscattering cone (the so called weak localization)[3, 4, 5]. Several experiments claimed strong localization of light in buck media [6, 7, 8], but these results are still today strongly debated [9, 10, 11, 12]. First Abdullaev in 1980[13] and then De Raedt in 1989 [14] proposed an alternative form of localization for light: the transverse localization. These authors described an optical system uniform in along the waves propagation direction, together with refractive index fluctuations distributed in the plane normal to propagation (transverse to it). In this case, starting from the Helmholtz equation[15] it is possible to obtain a paraxial equation for the slowly varying envelope of the optical field light, in which the temporal dependence is assumed to oscillate harmonically.

We report here the formulation form De Raedt and coworkers, which will be then harmonized with the recent results in the field of nonlinear optics. We start from the Helmholtz equation for the scalar field $\phi(\mathbf{r})$, which represents one of the components of the electric field $\mathbf{E}(\mathbf{r}, \mathbf{t})$

$$\phi(\mathbf{r}) + k_0^2 n(x, y)\phi(\mathbf{r}) = 0 \tag{1}$$

where $k_0 = \omega/c = \pi/\lambda$, ω is 2π times the frequency, c is the light velocity in the medium λ is the wavelength and $\mathbf{r} = [x, y, z]$. In the case of spatial longitudinal invariant system, the function $n(x, y)$ is the (transversely varying) refractive index. One can thus search solutions which have an oscillating envelope along z (the longitudinal direction) :

$$\phi(\mathbf{r}) = a(\mathbf{r}) \exp\left(-ik_0 n_0 z\right) \tag{2}$$

where n_0 is the average refractive index in the disordered medium (disordered fiber). Equation 1 becomes

$$-\frac{\partial^2 a(\mathbf{r})}{\partial^2 z}+2ik_0n_0\frac{\partial a(\mathbf{r})}{\partial z}=\frac{\partial^2 a(\mathbf{r})}{\partial^2 x}+\frac{\partial^2 a(\mathbf{r})}{\partial^2 y}+k_0^2[n(x,y)^2-n_0^2]a(\mathbf{r}). \tag{3}$$

By introducing a transversal nabla operator $\nabla_\perp=\frac{\partial^2}{\partial^2 x}+\frac{\partial^2}{\partial^2 y}$ and making the paraxial approximation [16]

$$\left|\frac{\partial^2 a(\mathbf{r})}{\partial^2 z}\right|<<2kn_0\left|\frac{\partial a(\mathbf{r})}{\partial z}\right| \tag{4}$$

Eq. (3) becomes

$$2ik_0n_0\frac{\partial a(\mathbf{r})}{\partial z}=[\nabla_\perp+U(x,y)]a(\mathbf{r}). \tag{5}$$

where the potential is defined by spatial distribution of he refractive index: $U(x,y)=k_0^2[n(x,y)^2-n_0^2]$. Equation 5 is formally equivalent to the Schrödinger equation driving electron localization[17]. In the case of the electromagnetic field propagating in the media for light, the role of time is played by the longitudinal coordinate z, while the role of potential is played by the refractive index distribution.

2 EXPERIMENTS ON TRANSVERSE LOCALIZATION

The first papers on localization where focused on theoretical modeling and numerical simulations. The experimental realization of the effect, required more than a decade from the paper of De Raedt and a several technological advances on the fabrication side. The difficulty relies in the realization of the propagation invariant disorder, which is particularly challenging at optical wavelengths, where it is need to realized "paraxial defetcts", (i.e. parallel scattering tubes) with sufficient precision in alignment, invariance along the symmetry axis for sufficient length and size comparable to that of light. The first approach to be successful was the"writing methods " based on photorefractive crystals, enabling to easily produce invariant system employing Gaussiam beams. On a second stage the TL has been realized employing fiber drawing technology, which enabled, longer structures, higher refractive indices, and exporting localization to an application-ready platform. In the last stage, TL met Femtosecond direct laser writing, which enables the direct control of the defects positioning enabling to investigate effects connected to the designed disorder. In the following we will describe all this.

2.1 Early experiments

The first experimental observation of TL (and actually one of the most unequivocal manifestation of light localization) has been reported by Schwartz and coworkers [18] employing photo-refractive media. The authors employed the optical induction technique, [19] to transform the intensity distribution of an array of parallel laser beams into a refractive index distribution thanks to the nonlinear response of the glassy material. The distribution of the beam intensity is controlled with an interference masks thus enabling the experimentalist to design the disorder configuration. The approach of Schwartz and coworkers induces a small refractive index change ($\Delta n\sim 10^{-4}$) and a large disorder grain size ($\sim 10\,\mu$m) thus the expected transport mean free path ℓ (the spatial length over which light propagation direction memory is lost) is large. The weak scattering regime resulting from the large ℓ, is expected to produce a large localization length ξ (the transversal section of the transmitting light tube) which, in principle, is detrimental for the observation of the localization phenomenon especially if ξ becomes larger than the transverse extension of the paraxial system. However this small (transverse) scattering strength is compensated by the very small transverse wavevector ($k_\perp=k_0\sin\theta$), with θ being the incidence angle, see the sketch in Fig. 1).

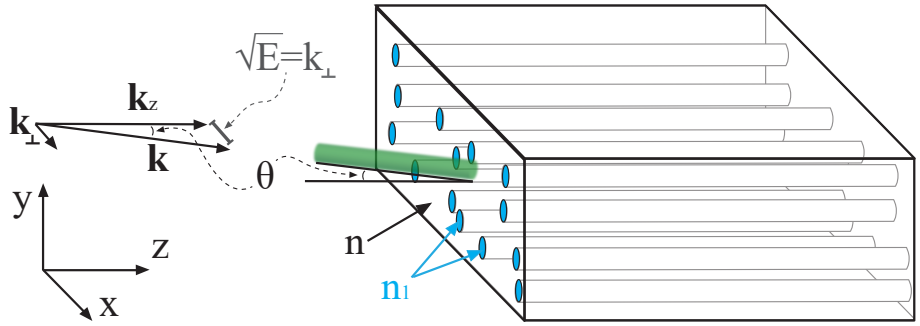

Figure 1. Sketch of transverse localization Sketch of the scattering structure and illumination for the realization of the TL. Light, in the form of a plane wave defined by the wavevector $\mathbf{k}$, is impinging on the sample, with an azimuthal angle θ. The projection of the wavevetor on the X, Y plane (parallel to the fiber facet) $\mathbf{k}_\perp$ and the projection of the wavevector on the propagation direction Z ($\mathbf{k_Z}$)are reported, together with the spectral parameter $\sqrt{(E)} = k_\perp$. The disordered system is typically consisting of a matrix of refractive index n containing "inclusions" with a different refractive index n_1. To work as "paraxial defects" the inclusions should be in the form of tubes parallel to Z.

The big advantage of the optical induction, is the possibility to completely rearrange the refractive index distribution, with a simple and fast rewriting procedure. The possibility to perform experiment with several realizations of the $n(x, y)$ enables to retrieve averaged-over-disorder quantities and this is a critical aspect to correctly assess the presence of light localization. In particular the author demonstrated a dependence of the localization length on the degree of disorder, thus demonstrating TL.

2.2 Optical fibers

In 2012, Arash Mafi and coworkers[20], demonstrated TL in a plastic optical fiber. They used a novel kind of fiber named *disordered binary fibers* (DBF), based on the random mixing of tens of thousands of plastic fibers of two types: poly-methyl-methacrylate and polystyrene. The two plastic were merged in random fashion and then, after the realization into a fiber-drawing tower, a single structure composed by a random puzzle of the two species was obtained. The binary fiber approach provides several advantages: i) the disordered refractive index distribution is permanent, ii) the refractive index mismatch between the two materials ($\Delta n \sim 0.1$) is orders of magnitude higher than in the case of optical lattices iii) the optical fibers are a mature technology ready for applications based on localization. Mafi and coworkers also fabricated glass optical fibers hosting transverse disorder and demonstrated TL therein [21]. The glass platform is extremely favourable for applications, providing very high refractive index contrast together with increased stability and lower absorption.

2.3 Image Transport

In-fiber implementation of the Anderson localization, enables the propagation of localized beams with the transverse size comparable to that of cores of commercial single mode optical fibers. Thus a single disordered fiber with sufficient transverse extension can act as a coherent fiber bundle [22]. In [23] Mafi and coworkers demonstrated image transport through disordered optical fibers up to 5 cm. The transported image quality is comparable to or slightly better than the one obtainable with commercially available multicore image fibres, with disorder reducing the pixelation effect present in periodic structures and improved contrast. On the other hand, the imaging resolution is limited by the quality of the cleaving and polishing of the fiber tip, while the transport distance is limited by the optical attenuation and the residual longitudinal disorder resulting form the imperfect drawing process. In this sense a glass based disordered

fiber, with an higher filling fraction and much lower losses has the potential to further improve endoscopic disordered fibers.

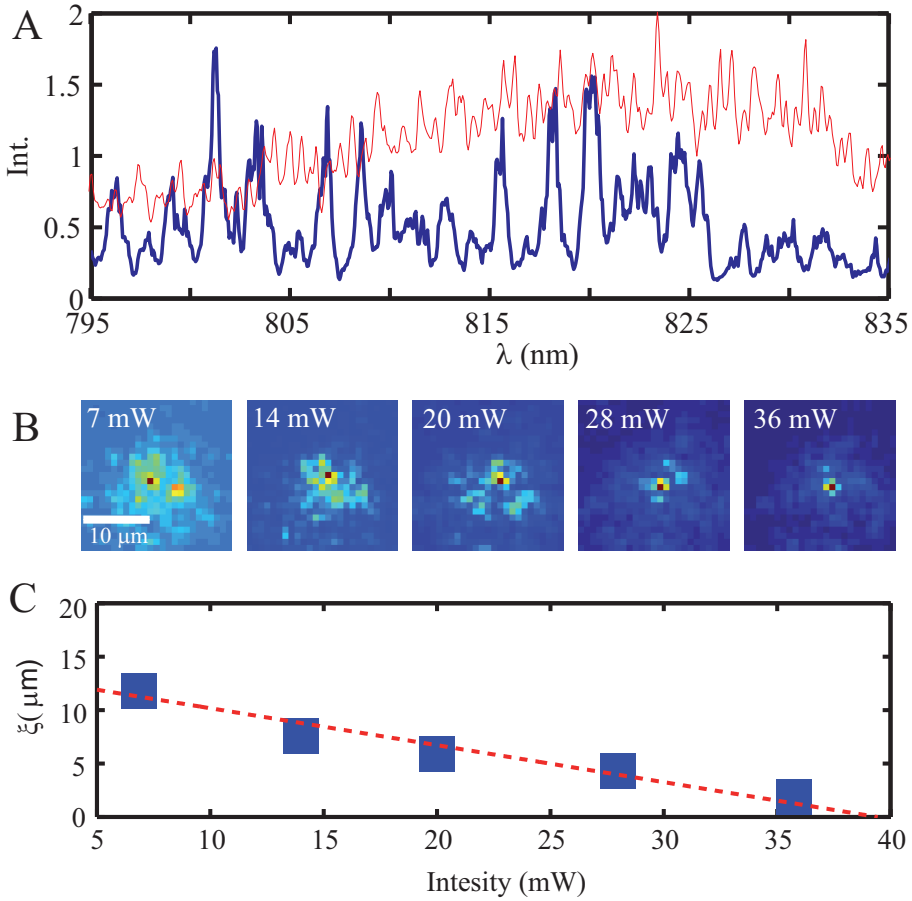

Figure 2. Localized states and nonlinearity Panel A reports the spectrum (blue thick line) retrieved at the output of a disordered fiber (the collection area is 1 μm). The red thin line represents the source spectrum. Panel B reports the shape of the most intense mode (at ≃801 nm), for five values of the input power. Panel C Shows localization length versus input intensity. All data are from [24].

2.4 Nonlinearity in disordered optical fibers

There is a relevant debate about the fact that nonlinearity [25, 26] may enhance disorder induced localization. The interplay between disorder and a nonlinear response may strongly modify the process of disordered induced wave trapping in TL. In particular in the case of nonlocality, while localization tend to reduce the inter-mode interactions, a nonlinear perturbation, extending beyond the region of the localized state, could eventually produce some kind of action at a distance. The first experimental evidence of non-localitiy acting together with Anderson localization in an optical fiber, has been shown in [24]. In that paper, the disordered fiber has been probed with a broadband laser beam, showing a distribution of sharp peaks in the transmittance, as expected from the "resonant" behavior of the disorder induced localized states (in Fig. 2a we report the spectrum transmitted from the fiber (blue) compared to the probe spectrum (red)). The first evidence is that the spatial shape of the localized states is strongly affected by energy probe beam power. This effect is reported in panel. 2b,c where the localized state shape is reported as a function of the input power. The mode is seen to shrink when power is augmented.

This self focusing results from the peculiar interaction between disorder and thermal nonlinearity. In general, the refractive index of a nonlinear optical material, varies with the optical intensity I as $n = n_0 + \Delta n(x, y) + n_2 I$, where $\Delta n(x, y)$ is the refractive index fluctuation due to disorder and n_2 represent the coefficient of the nonlinear perturbation. A positive n_2 coefficient results in a converging wave front that can potentially surpass the diffraction limit. Conversely, a negative value of n_2 produces a de-focusing nonlinearity, thus the expansion of the beam. In plastic binary fibers, one expects the slow thermal nonlinearity to yield a negative n_2 thus de-focusing. However experimental measurements report instead a focusing nonlinerarity. This unexpected effect is explained in reference [27]. In practice, if the refractive index reduction is more pronounced in one of the two constituent materials of the binary fiber, the refractive index mismatch may increase. Thus the overall refractive index reduction is compensated by a stronger localization (smaller mean free path due to the refractive index mismatch enhancement). This effect enables a local and optical tunability of the localization length, enabling to drive the position of the localized states in a form of localization-mediated beam steering. The steering effect is reported in Fig. 3. Panel 3A, shows light reflected by the fiber input: the probe beam (green spot on the left) and the pump beam (red spot on the right) present. Panels 3B-D show the shape of the probe beam at the output as a function of the pump beam power.Here it is possible to note how much the probe beam is attracted towards the pump one Panel 3E shows the distance of the probe beam center as a function of the input power.

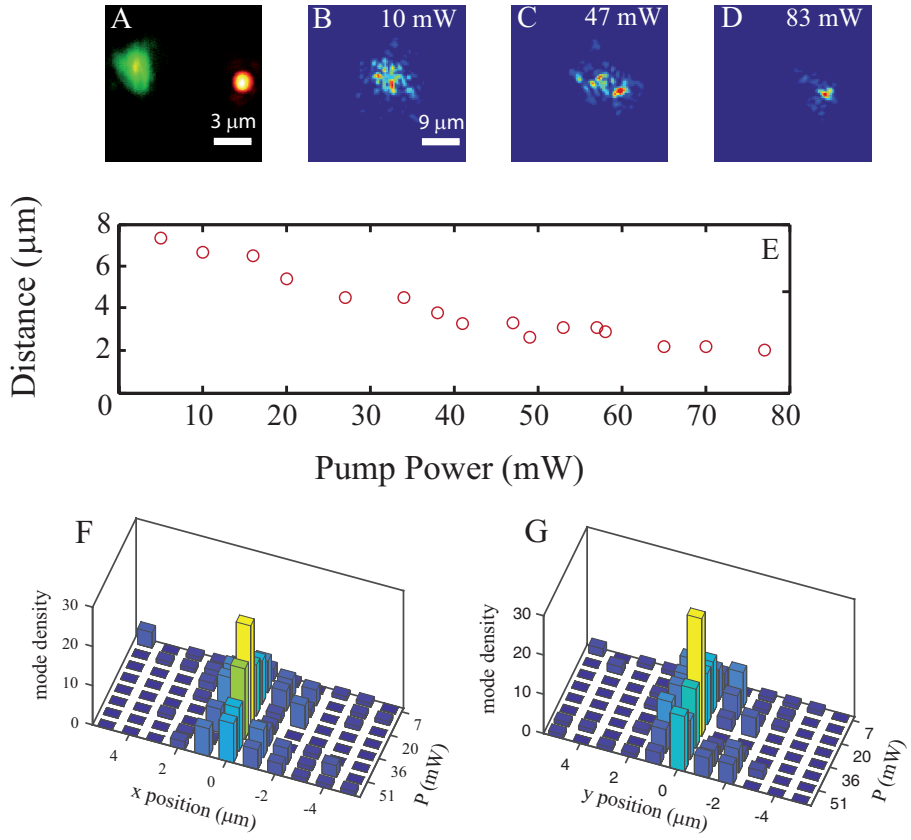

Figure 3. Light steering in the localization regime. Panel A shows the input of the DBF, showing the probe beam (green on the left) and the pump beam (red on the right) . Panels B-D report the probe beam (pump light has been removed from the detector with a spectral filter) for several values of pump power. Panel E shows the distance between probe and pump beam versus the pump power. Panels F-G, report the modes density along the X axis and Y axis (respectively) and for several pump powers. Data from [24].

Nonlocality obviously works also when more than two modes are involved. The behaviour of a group of localized modes is visualized in panel 3F,G. Here we show (data from [24]) the mode density (number of localized modes per square μm) along the x and y axis at the output of a fiber. The mode density has been characterized for various values of the input power. The modes indeed appear to be attracted one another and then after a "collision" they start to diverge. Following an approach very similar to that already developed for solitons [28, 29], in the case of a nonlinear medium it is possible to write down a nonlinear version of equation 5:

$$-2ik_0n_0\frac{\partial a(\mathbf{r})}{\partial z} = [\nabla_\perp + 2k_0^2\Delta n]a(\mathbf{r}). \tag{6}$$

where $\Delta n(x,y) = \Delta n_r(x,y) + \Delta n_{NL}(x,y)$, and the nonlinear part of the refractive index may be approximated as $n_{NL}(x,y) = P(\Delta n_1 + \Delta n_2|\mathbf{r} - \mathbf{r}_L|^2/2)$ where $\mathbf{r}_L$ is the transverse position of the localized state indexed with L ($L = 1, 2....N$ with N the total number of localized states). By searching solutions of the kind $a(x,y,z) = \tilde{a}(x,y)\exp(i\beta z)$, eq. 6 becomes

$$\frac{1}{k_0n_0}\nabla_\perp\tilde{a} - k\Delta n_L\tilde{a} = (\beta + k\Delta n_1 P)\,\tilde{a}. \tag{7}$$

where we introduced the input power P and the linear index perturbation coefficient Δn_L. Thus the effect of nonlinearity is that to shift the eigenvalues with respect to the their linear value β_L. The power dependant eigenvalue is thus $\beta(P) = \beta_L - k_0\Delta n_L$. This shifting reflects on the localization length ξ in the form

$$\xi(P) = \xi(0)(1 - \frac{P}{2P_c}) \tag{8}$$

with the critical power $P_C = |\beta_L|/(2k\Delta n_1)$.

To model the power dependent spatial displacement of modes, we can resort to the general Ehrenfest theorem of quantum mechanics stating that for the Hamiltonian $H = \frac{p^2}{2m} + V(x)$ the relation $m\frac{\partial^2\langle x\rangle}{\partial t^2} = -\left\langle\frac{\partial V(x)}{\partial x}\right\rangle$ (the quantum mechanical equivalent of the Newton law) holds. Applying it to Eq. (6) it is possible to cast an equation for the positions of the localized states:

$$P_L\frac{\partial^2\mathbf{r}_L}{\partial z^2} = \int I_L(\mathbf{r} - \mathbf{r}_L)\nabla_{x,y}\frac{\Delta n_{NL}}{n_0}d\mathbf{r} \tag{9}$$

In Eq. (9), $I_L(\mathbf{r} - \mathbf{r}_L)$ is the intensity profile of a localized state, $\nabla_{x,y} = \frac{\partial}{\partial x} + \frac{\partial}{\partial y}$ and $P_L = \int I_L(\mathbf{r} - \mathbf{r}_L)d\mathbf{r}$ plays the role of mass in a Newtonian system. As the various localized states are incoherent (appear at different wavelengths), thus Δn_{NL} can be written as the sum of the individual perturbation produced by each state:

$$\Delta n_{NL} = \sum_{l=1}^{N}\Delta n_{NL,l} \simeq \sum_{l=1}^{N}P_l(\Delta n_1 + \frac{\Delta n_2}{2}(\mathbf{r} - \mathbf{r}_l)^2). \tag{10}$$

where the n_2 behaviour has been approximated with a parabolic behavior (Taylor series) with respect to the spatial coordinate centered in the localization positions $\mathbf{r}_l$. Now we recall that the intensity distribution

of each localized state $I_L(\mathbf{r}-\mathbf{r}_L)$ is much sharper than the profile of the thermally induced refractive index modification spatial extension $\Delta n_{NL,l}$ thus we are allowed to treat it as a Dirac δ with area P_L. Using 10 into 9 we obtain:

$$P_L \frac{\partial^2 \mathbf{r}_L}{\partial z^2} \simeq -\nabla_{x_L,y_L} \sum_{l=1}^{N} -\frac{|\Delta n_2| P_L P_l}{2n_0} |\mathbf{r}-\mathbf{r}_l|^2 \tag{11}$$

in which the constant therm Δn_1 has been discarded due to presence of the ∇_{x_L,y_L} operator. Equation 11 is a gravitation-like equation for the localized states. It predicts a pairwise, attractive, force between each localized light tube. The force strength is proportional to the product of their power in the same way the in gravitational force it is proportional to the product of masses. The more intense localized states will attract the smaller ones, thus tending to collapse to a specific point. Being the system conservative after the interaction the forces will spread again as shown in panels 3F and 3G.

2.5 Localized states and "single modes"

The Anderson localization (AL) scenario typically comprises a disordered system supporting states which are strongly localized at different locations in space and at different energies [30]. These disorder induced resonances, have thus a poor or negligible spatial and spectral overlap so that transverse energy transport is substantially slowed down.

While the majority of the studies on AL are focused on the measurement of transport related quantities (such as diffusion or conductance [6, 7, 8, 32]), it is also interesting to study the properties of disorder-generated localized state. These light structures could be employed for energy storage[33, 26] or super efficient lasing [34, 35]. Indeed localized states act exactly like a microresonator, with the difference that the resonance is sustained by a disordered structure instead of a regular one. In photonics this kind of "lonely" structures are extensively employed in several fields: the most successful applications are in the field of fiber optics and laser resonators where they are named single mode resonators or single mode fibers. The principle of operation is for both applications very similar: they are resonant structure designed to host a single solution (typically the fundamental one) of the wave equation without (or with very small) losses.

In the case of disordered optical fibers one may ask, to which extent a localized state operates as a single mode hosted in the core of single-mode fibers. This issue has been extensively studied in [31].

In contrast to multi-mode fibers, disordered binary fibres (DBF) show peculiar transmittance maps. The transmittance map is the total (integrated over the whole fiber tip output) intensity measured as a function of the injection location, and measured with the setup shown in Fig. 4. Light form a CW laser is tightly focused into a 0.7 µm diameter spot at the DBF input. The fiber input tip is sustained by a motorized actuator which enables to scan the injection location ($\mathbf{r}=[x,y]$) along the input plane. The total transmittance $T(\mathbf{r})$, is thus obtained summing the whole intensity measured on the output plane ($\mathbf{R}=[X,Y]$) by Camera 2. A typical transmittance map is reported in panel 4A. It is possible to note that high transmittance locations (green spots) are appearing in sparse fashion and surrounded by a sea of barely transmitting locations. These "hotspots" are the locations at which the input (which has a size much smaller than the the localization length), couples efficiently to a transmission channel corresponding to a transversely localized state. The fact that the transmittance map is sparse should be thus a consequence of the fact that the coupling condition are very "strict" (resonance bandwidth is very small) and thus coupling happens only at specific locations.

Now it is interesting to further investigate the nature of these transmittance hotspots. The most accessible feature is the intensity profile measured at the fiber output: this is reported at Fig. 5 for four different input

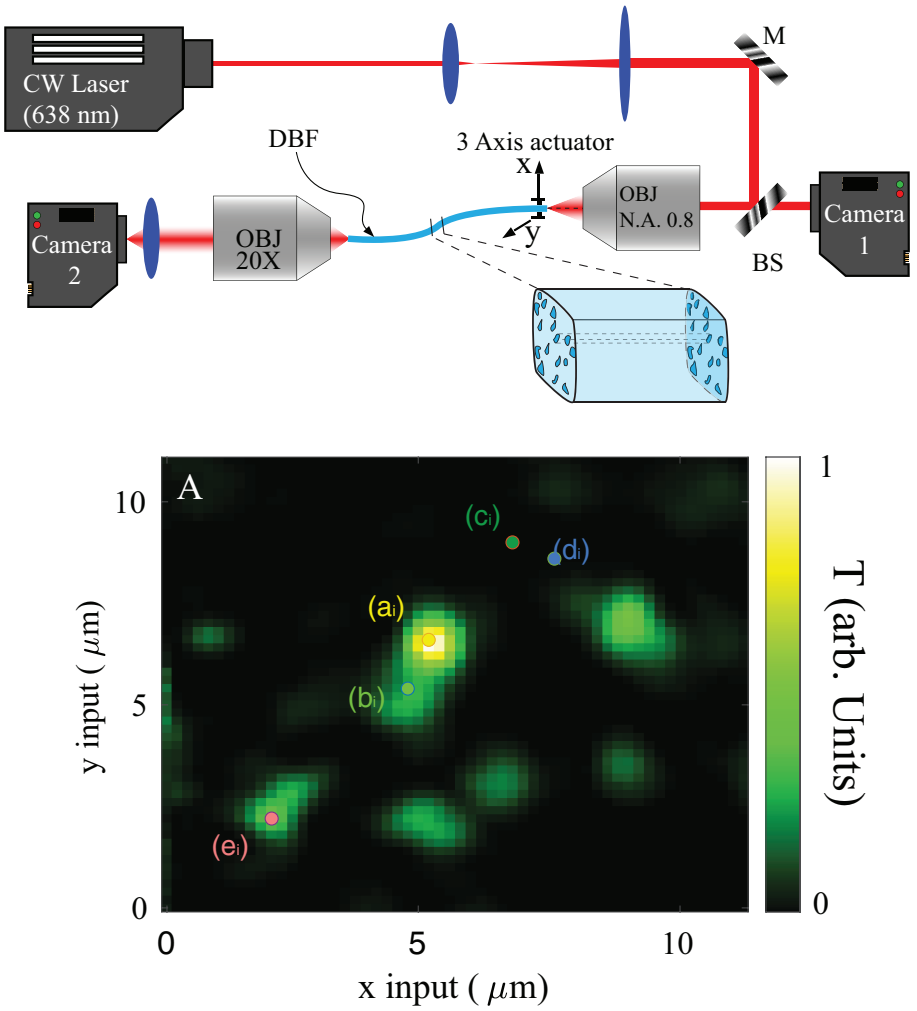

Figure 4. Probing single mode nature of localized states The sketch reports a scheme of the experimental setup. Legend: CW laser - continuous wave laser; M - Mirror; BS - beam-splitter; OBJ - objetcive; DBF - disordered binary fiber. Panel A reports the transmittance map in a 10 μm side field of view. Data from [31].

locations. The input locations are identified by small colored dots labeled (a_i b_i,c_i, d_i) in Fig. 4A. The intensity profiles 5B and 5C correspond to injection locations in the same hotspot and they produce two very similar output intensity profiles. On the other hand, two very close input locations lying in a barely transmitting area (5C and 5D) produce two very different output intensity profiles. The intensity profile corresponding to an high efficient transmission channel is thus a fingerprint of the channel. In the same way the Gaussian profile going out from a single mode fiber is an indistinguishable signature for efficient coupling of a laser beam to the fundamental mode of the fiber's core.

To verify this picture, one should observe where the mode's fingerprint is found while scanning the input of the fiber. To perform this measurement systematically, the authors engineered a specialized observable that is the Degree of Similarity $Q(r_1, r_2)$

$$Q(r_1, r_2) = \int I(R, r_1) I(R, r_2) dR \tag{12}$$

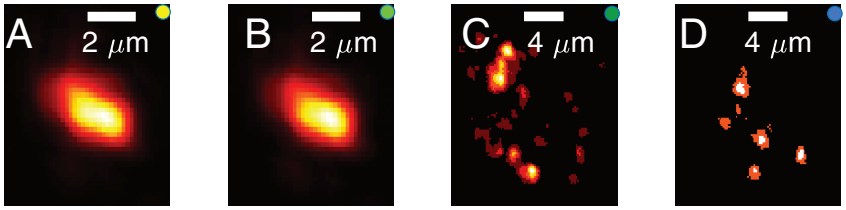

Figure 5. Mode Fingerprints Each Panel reports the spatial profile of the intensity found for the correspondent location in Fig. 4: i.e. panel A shows the fingerprint for location (a), B for location (b) ecc. Data from [31].

normalized such that $Q(r,r) = 1$. The fingerprint of a transmission channel is the output intensity profile retrieved at the location of higher transmittance. So for the transmission channel located at a_i produces a Q-map $Q(r_a, r_2) = \int I(R, r_a) I(R, r_2) dR$, where r_a corresponds to location of higher intensity of the mode a_i. By computing $Q(r_a, r_2)$ for all r_2 in the field of view, we retrieve the Q-map reported in Fig. 6A. The white/bluish area (where $Q \simeq 1$) corresponds to the dwelling area of the mode: the set of input locations from which the mode can activated. The dwelling area is very sharp, meaning that when the mode is activated no other modes (which would modify the fingerprint and immediately lower the Q) are activated.

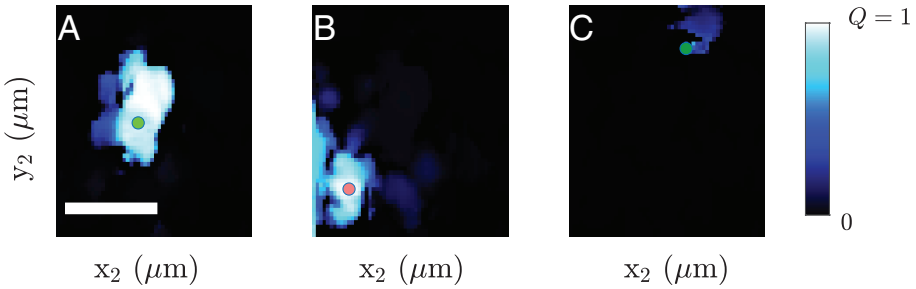

Figure 6. Q-maps Panels A, B and C show Q-maps for modes (a) (e) and (c) respectively. Data from [31].

A similar picture is found in Fig. 6B for the mode in e_i. The two modes are only barely overlapping: energy is not flowing from one degree of freedom to the other. The dark area in both maps corresponds to locations in which no intensity is transferred to the localized state. Note that the small displacements of the input inside the dwelling area the do not cause any modification in the mode fingerprint. Multi-mode light structures, would give rise to a pronounced flickering of the image due to the difference in phase delay over different modes summing in different fashion when input is displaced. The absence of such flickering is a relevant proof of the single-mode nature of the light structures supported by the DBFs.

On the other hand Fig. 6C, related to mode (c_i), provides a Q-map almost entirely empty: in absence of a transmission channel, retrieved light is not coupled to a localized state. In this case the fiber behaves in way similar to a (very leaky), large-core multi-mode fiber where a small translation of the input produces a complete change of the output due to interference (thus an immediate decay of the Q value). Thus: i) high transmission channels in a DBF are sparse; (ii) they are separated by a barely transmitting "sea" ;(iii) independently on how (and where) light is coupled to a DBF each transmission channel retains its

fingerprint (output profile); (iv) modes are excited in alternative fashion (i.e the same input location activates only a transmission channel at time). In other words localized states of a DBF behave exactly how single modes from single mode fibers showing the same property: the "resilience to the launch conditions".

2.6 Designed disorder in Glass fibers

Disorder binary fibers (DBF) are an unique architecture, [36]: a fiber without cores (thus similar to a multmode fiber) , capable to host localized/single mode solutions. However, the high absorbance of the plastic component materials, together with fabrication-induced scattering losses, degrades consistently their transmittance efficiency, which remains very limited especially if compared with the properties of silica fibers capable to transmit light for kilometer with few losses. It is thus very promising to obtain TL on disordered glassy fibers. The first observation of transverse Anderson localization in a glass optical fiber has been obtained by Mafi and coworkers [21]. The glassy disordered fiber has been obtained, in that case starting form a "porous satin quartz" rod of 8 mm in diameter and 850 mm in length from which a single 150 m long fiber (diameter 250 µm) has been obtained. In this system, the non homogeneous distribution of disorder (lower air hole density in the fiber central region), produces localized states only at the borders of the fiber. This uneven distribution of disorder forbids a complete optical exploitation of the waveguide section. Moreover the positions of the defects (the air bubbles) is random (it results from the natural occurrence of pores in the rod) and cannot be tuned by the user at the fabrication stage.

On the other hand the concept of designed disorder [37] is becoming an intense field of research with applications ranging from the fabrication of waveguides, polarizes or to light harvesting [38, 39, 40]. In fact, in some cases, disordered structures or solution, even if fully deterministic, can be more favourable in specific tasks than periodic ones. For example, disordered arrays of defects can be employed to produce a structure displaying different propagation regimes, (full photonic bandgap, Anderson localization or free diffusion) depending on the wavelength employed [41].

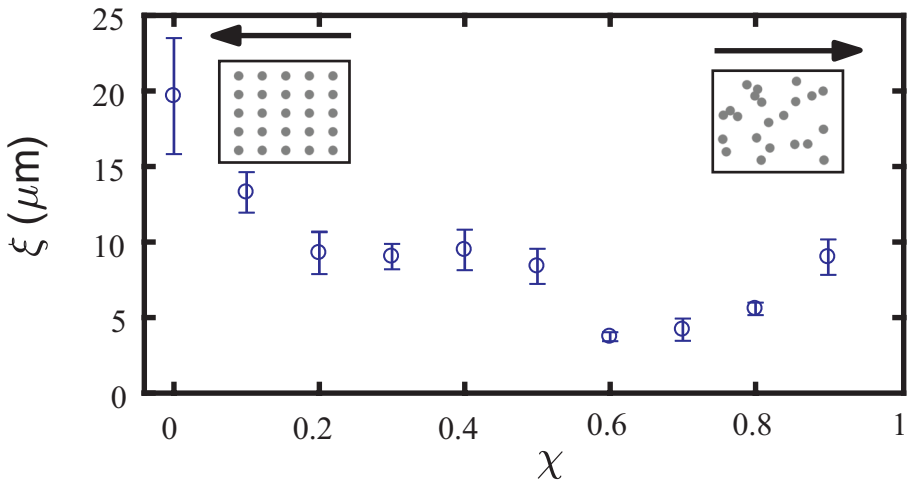

Figure 7. Localization length in Direct laser written disorder Localization length ξ versus degree of disorder χ, measured in a D Glassy substrate in which paraxial defects have been realized with FDLW. Data from [42].

In order to implant "designed disorder" into glassy optical fibers, the authors of [42] employed the femtosecond direct laser writing (FDLW) technique. FDLW [43] exists since early nineties, and enables nanometric resolution in surface ablation. In in transparent materials, bulk micro machining can be achieved trough nonlinear (two or three photon) absorption thus enabling the fabrication of photonic or microfluidic

devices. The strong confinement of the nonlinear absorption volume, together with positioning performed by piezo-actuators with nanometric resolution, enables the fabrication of three-dimensional and complex structures. The modifications by nonlinear absorption yield local refractive-index change (at low power) or even void formation (at high power). Importantly the changes produces are permanent, thus the low power approach enables to produces durable wave guides. The group of A. Szameit and coworkers reported several experiments on waveguide arrays in which disorder is introduced in the inter-waveguide coupling factors. This approach enabled to investigate Anderson localization [44, 45, 46, 47], defect localization [48], and also topological insulation [49]. This wave-guide based approach, indeed, enables to access a plethora of intriguing physical phenomena, however it requires the individual fabrication of each of the transmission channels. In this sense DBF support localization in a different manner: they can be, indeed, seen as a continuous meta-material, potentially hosting localized states at any location, which could support the resonance condition. The most evident consequence of this difference is that localized states translate gradually their position when wavelength is changed in DBF, while they can be hosted only at the waveguides location in waveguides-arrays.

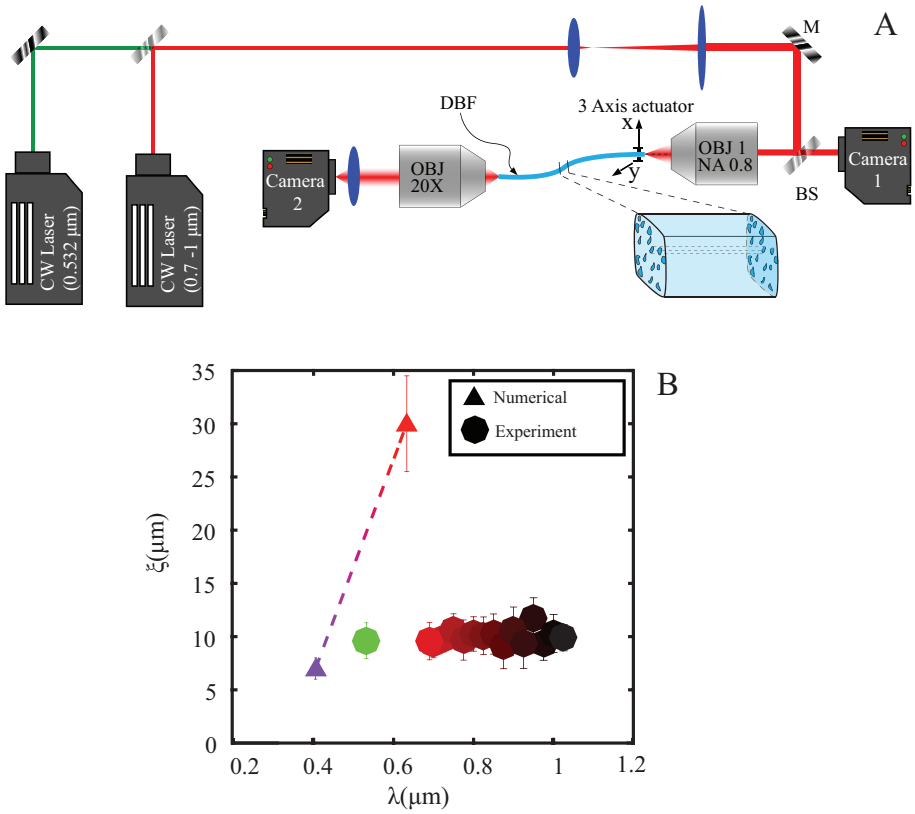

Figure 8. A) The experimental setup is an evolution of the one shown in Fig. 4, in which probe beam is generated either by a tunable laser (tunability range 0.690 µm and 1.04 µm) or at a fixed wavelength (532 nm) laser. The back-reflected light is then visualized by the camera CCD1 through the beam-splitter (BS) to focus the beam at the fiber entrance. The piezo devices control the laser injection location. The transmitted light is collected by the objective OBJ2 ad imaged on camera CCD2 with a magnification of $\times 50$. Panel B reports localization length ξ versus wavelength λ for both numerical simulations and experiments. Experimental data are from [50] while numerical data are from [51].

In order to transfer the advantage of DBF to glasses Gianfrate and coworkers [42], employed FDLW in a a non-traditional way. In particular they employed an objective with high numerical aperture (NA=0.65)

to generate very small diameter tubes with refractive index larger than the surrounding medium. These paraxial structures play the role of a transversal scatterer, because their reduced transverse dimension does not enable to support propagating modes: they act as paraxial defects (see sketch in Fig. 1). This new generation of optical fibers based on paraxial defects have been studied in [42], where the authors show how the localization strength depends on the degree disorder properties. The authors demonstrate that the confinement properties depend on the degree of disorder $0 < \chi < 1$: a parameter tuned at the fabrication stage. The paraxial defects are fabricated at the transverse coordinates $[X_{M_x}, Y_{M_y}] = [\delta(M_x + \chi\theta_{M_x}), \delta(M_y + \chi\theta_{M_y})]$, where M_x and M_y are integer numbers Between 0 and S, δ is the lattice size and θ is an uniform random number between [-0.5 and 0.5]. When χ is 0 the paraxial defects are located in a square lattice with cell side δ and S^2 defects (square with side δS). For $\chi > 0$ each defect is displaced of a random amount $\delta\chi\theta_{Mx}$along X and $\delta\chi\theta_{My}$ along y, generating a square lattice with an increased degree of randomness. Fig. 7 reports the measured localization length ξ as a function of χ. It is possible to note that the localization length decreases up to 0.6 and then starts to increase again. While the decrease is naturally expected as a natural consequence of increasing disorder, the increasing behaviour above $\chi = 0.6$ is resulting from the appearance of overlapping paraxial defects which are effectively decreasing the defect density.

The realization of localization induced by direct laser written defects is the fist step for a new generation of glass based optical fibers characterized by low absorption and greater stability with respect to their plastic counterpart. The possibility to directly tune the defect position will open the possibility to test the concepts of designed disorder directly in optical fibers, thus paving the way towards potentially disruptive applications.

2.7 Experimental verification of the theory of Anderson localization

The traditional theoretical description of Anderson localization of light, and, in particular, transverse Anderson localization [51, 52] predicts a pronounced dependence of the localization length on the of the light wavelength. This is implied by the dependence of the potential $U(\mathbf{r})$ in Eq. (5) on $k_0 = 2\pi/\lambda$. The authors of [50] investigated this effect experimentally (see a sketch of the setup in Fig. 8A) in order to verify the validity of the current theory of Anderson localization of light. The experimental setup is shown in Fig. 8. Panel 8B reports the the localization length ξ versus the incident-laser wavelength: no dependence on the wavelength is retrieved in the range $0.55\,\mu\text{m} \leq \lambda \leq 1\,\mu\text{m}$. The explanation of this discrepancy with the theoretical predictions will be fully explained in the following section, where a comprehensive and correct theory of transverse Anderson localization of light in optical fibers is presented.

3 THEORY OF TRANSVERSE ANDERSON LOCALIZATION OF LIGHT

3.1 Wave equation for electromagnetic waves in a disordered environment

As indicated in the introduction, almost the entire literature on Anderson localization (AL) of light is based on the potential-type wave equation, i.e. a wave equation in which the spatially fluctuating permittivity $\epsilon(\mathbf{r})$ appears as a coefficient of the double-time derivative of the wave function (electric field). In a recent article [50] we have shown that this wave equation is in error and leads to a fictitious wavelength dependence of the localization length in transverse localization, which is not observed in the experiments. We now review the derivation of the traditional wave equation, show, which error was made and present the derivation of the correct wave equation.

Maxwell's equations in a medium with spatially varying permittivity $\epsilon(\mathbf{r})$ are

$$\nabla \cdot \mathbf{B}(\mathbf{r},t) = 0 \qquad \nabla \cdot \mathbf{D}(\mathbf{r},t) = 0 \qquad \mathbf{D}(\mathbf{r},t) = \epsilon(\mathbf{r})\mathbf{E}(\mathbf{r},t) \tag{13a}$$

$$\nabla \times \mathbf{B}(\mathbf{r},t) = \frac{1}{c^2}\frac{\partial}{\partial t}\mathbf{D}(\mathbf{r},t) \qquad \nabla \times \mathbf{E}(\mathbf{r},t) = -\frac{\partial}{\partial t}\mathbf{B}(\mathbf{r},t) \tag{13b}$$

For deriving a wave equation for the electromagnetic fields one can either solve for the electrical field $\mathbf{E}(\mathbf{r},t)$ or for the magnetic field $\mathbf{B}(\mathbf{r},t)$. The traditional procedure (potential-type approach, PT) was to solve for $\mathbf{E}(\mathbf{r},t)$:

$$\begin{aligned} \frac{\epsilon(\mathbf{r})}{c_0^2}\frac{\partial^2}{\partial t^2}\mathbf{E}(\mathbf{r},t) &= -\nabla \times \nabla \times \mathbf{E}(\mathbf{r},t) \\ &= \nabla^2\mathbf{E} - \nabla\big(\nabla \cdot \mathbf{E}(\mathbf{r},t)\big) \\ &\approx \nabla^2\mathbf{E}\,, \end{aligned} \tag{14}$$

where, in the last step $\nabla \cdot \mathbf{E} = 0$ was assumed. In the frequency regime we obtain the following stochastic Helmholtz equation

$$-\omega^2\frac{\epsilon(\mathbf{r})}{c_0^2}\mathbf{E}(\mathbf{r},\omega) \approx \nabla^2\mathbf{E}\,, \tag{15}$$

which, separating the fluctuations of the permittivity as $\epsilon(\mathbf{r}) = \langle\epsilon\rangle + \Delta\epsilon(\mathbf{r})$, can be rewritten as

$$\omega^2 \frac{\langle\epsilon\rangle}{c_0^2}\mathbf{E}(\mathbf{r},\omega) \approx \Bigg(-\nabla^2 + \underbrace{\omega^2 \frac{-\Delta\epsilon(\mathbf{r})}{c_0^2}}_{\mathcal{V}(\omega)} \Bigg)\mathbf{E}(\mathbf{r},\omega) \tag{16}$$

Replacing the electric field $\mathbf{E}(\mathbf{r},\omega)$ by a scalar field ϕ and introducing k_0 as $k_0 = \sqrt{\langle\epsilon\rangle}\omega/c_0$ we recover Eq. (5). As said in the introduction, this equation is mathematically equivalent to a stationary Schrödinger equation for an electron in a frequency-dependent random potential $\mathcal{V}(\omega)$. This equivalence made it possible to transfer the complete electronic theory of AL [32, 53] to classical electromagnetic waves [54, 55, 56, 57]. We call this approach "potential-type" (PT).

We now want to check the validity of the approximation made in Eqs. (14) to (16) We have

$$0 = \nabla\cdot\mathcal{D} = \nabla\cdot\Big(\epsilon(\mathbf{r})\mathbf{E}(\mathbf{r})\Big) = \epsilon(\mathbf{r})\nabla\cdot\mathbf{E}(\mathbf{r}) + \mathbf{E}(\mathbf{r})\cdot\nabla\epsilon(\mathbf{r}) \tag{17}$$

from which follows [58]

$$\nabla\cdot\mathbf{E} = -\frac{1}{\epsilon(\mathbf{r})}\mathbf{E}\cdot\nabla\epsilon(\mathbf{r}) \neq 0 \tag{18}$$

One can estimate the error made in (14) by inserting for $\mathbf{E}$ a wave with wavelength λ. If the scale, on which the permittivity is varying, is large with respect to λ (eikonal limit), the term on the right-hand side of (18) is negligible. However, if this condition is fulfilled, one deals with very weak disorder. In this case one has in three dimension delocalization, and in two dimension a very large localization length, exceeding macroscopic sample dimensions, which would make the observation of AL impossible. So, for stronger disorder, where one might have a chance for observing AL, the scale of the permittivity fluctuations must be of order λ. In this case the divergence of $\mathbf{E}$ is not negligible. This renders the approximation made in the PT wave equation (14) invalid.

On the other hand, if we solve the Maxwell equations (13a) for $\mathbf{B}$ we obtain (using $\nabla\cdot\mathbf{B}(\mathbf{r},t) = 0$)

$$\frac{\partial^2}{\partial t^2}\mathbf{B}(\mathbf{r},t) = -\nabla\times\frac{c_0^2}{\epsilon(\mathbf{r})}\nabla\times\mathbf{B}(\mathbf{r},t) = \nabla\cdot\frac{c_0^2}{\epsilon(\mathbf{r})}\cdot\nabla\mathbf{B}(\mathbf{r},t) \tag{19}$$

Eq. (19) leads to the following stochastic Helmholtz equation

$$-\omega^2\mathbf{B}(\mathbf{r},\omega) = \nabla\cdot M(\mathbf{r})\cdot\nabla\mathbf{B}(\mathbf{r},\omega)\,, \tag{20}$$

where we have defined the spatially fluctuating dielectric modulus as $M(\mathbf{r}) = c_0^2/\epsilon(\mathbf{r})$.

Eq. (20) is mathematically equivalent to the Helmholtz equation for an elastic medium with zero bulk modulus and a spatially fluctuating shear modulus $M(\mathbf{r})$. This equation is exact and is called the modulus-type (MT) approach[1]. A theory for a medium with finite (constant) bulk modulus K and a spatially fluctuating shear modulus has been worked out [59, 60, 61] by some of the present authors and applied for explaining the anomalous vibrational properties of glasses, in particular the enhancement of the vibrational density of states with respect to the Debye law ("boson peak"). Our present theory of Anderson localization

[1] Because of the relation (18) there is no analogous equation for $\mathbf{E}(\mathbf{r},\omega)$. The corresponding equation, which involves the local gradients of $M(\mathbf{r})$, is much more complicated.

of light relies on the analogy to this case. Essentially one needs only to take the $K \to 0$ limit for this theory and obtain a theory for light diffusion and localization in disordered optical systems.

In order to describe transverse Anderson localization we first map this problem to a two-dimensional problem. We then use the paraxial approximation to map the z dependence of the wave profiles to the time dependence in an effective Schrödinger equation. For estimating the diameter of the large-z profile, the localization length ξ we apply the scaling theory of Anderson localization [62, 32], which is equivalent to the renormalization-group approach to the generalized nonlinear sigma model [63, 64, 65]. For the calculation of the z dependence of the localization length we then use the self-consistent localization theory of Vollhardt and Wölfle [53, 66, 67, 57].

3.2 Description of optical fibers with transverse disorder

We now consider an optical fiber with transverse disorder, i.e. the permittivity exhibits spatial fluctuations in x and y direction, but not in z direction. Without of loss of generality we may replace the vector $\mathbf{B}(\mathbf{r},\omega)$ by a scalar $B(\mathbf{r},\omega)$. In our treatment the vector character of the wave function only enters into the sum over modes, where one has to insert a factor of two.

Because our system is translation invariant with respect to the z direction we may take a Fourier transform with respect to z: $B(\boldsymbol{\rho},k_z,\omega) = \int dz e^{ik_z z} B(\boldsymbol{\rho},z,\omega)$, where $\boldsymbol{\rho} = (x,y)$ is the position vector in the transverse plane. We then obtain an effective two-dimensional Helmholtz equation

$$\left(\underbrace{[k_0^2 - k_z^2]}_{\mathsf{E}} + \nabla_{\boldsymbol{\rho}} \cdot \frac{M(\boldsymbol{\rho})}{\langle M \rangle} \cdot \nabla_{\boldsymbol{\rho}} \right) B(\boldsymbol{\rho}, k_z, \mathsf{E}) = 0 \tag{21}$$

Here $k_0 = \omega/\sqrt{\langle M \rangle} = 2\pi/\lambda$ is the wavenumber of the input laser beam, λ is its wavelength, and θ is the angle between the direction of the incident beam direction and the optical axis (azimuthal angle), see Fig. 1. $\mathsf{E} = k_0^2 - k_z^2 = k_\perp^2 = k_0^2 \sin^2\theta$ is called the spectral parameter. It replaces the spectral parameter ω^2 of a true two-dimensional system.

For $\theta \ll 1$ we can make the approximation $E = (k_0 + k_z)(k_0 - k_z) \approx -2k_0(k_z - k_0) \equiv -2k_0 \Delta k_z$, which is equivalent to the *paraxial approximation* [68], introduced in the introduction. The wavenumber Δk_z refers to the Fourier component of the *envelope* $A(\rho,z) = B(\rho,z)e^{-ik_0 z}$, which describes the beats of the wave function $B(\rho,z)$ in z direction. In the paraxial limit $A(\rho,z)$ obeys the paraxial equation

$$\left(i\frac{\partial}{\partial \tau} + \nabla \cdot \frac{M(\boldsymbol{\rho})}{\langle M \rangle} \cdot \nabla \right) A(\rho,\tau) = 0\,, \tag{22}$$

where the "time" $\tau = z/2k_0$ has the timension of a squared length. Eq. (22) is equivalent to the Schrödinger equation of an electron in a medium with a randomly varying *effective mass*. It is related to a stochastic tight-binding model with a spatially fluctuating hopping amplitude ("off-diagonal disorder") [69].

3.3 Mean-field theory for wave propagation in a turbid medium

3.3.1 Average Green's function and self-consistent Born approximation (SCBA)

We now assume that the fluctuations $\Delta(\boldsymbol{\rho}) = -\big[M(\boldsymbol{\rho}) - \langle M \rangle\big]/\langle M \rangle$ of the local moduli are Gaussian distributed with probability density

$$P[\Delta(\boldsymbol{\rho})] \propto \exp\left\{ -\frac{1}{2\gamma} \int \frac{d\boldsymbol{\rho}}{A_c} \Delta(\boldsymbol{\rho})^2 \right\} \tag{23}$$

with $\gamma = \mathsf{Var}[\Delta(\boldsymbol{\rho})]$, and A_c is an area proportional to the square of the correlation length ℓ_c of the fluctuations.

The Green's function corresponding to the stochastic wave equation (21) obeys

$$\Big[s - \nabla_{\boldsymbol{\rho}} \cdot \Big(1 - \Delta(\boldsymbol{\rho})\Big) \cdot \nabla_{\boldsymbol{\rho}}\Big)\mathsf{G}(\boldsymbol{\rho}, \boldsymbol{\rho}', s) = -\delta(\boldsymbol{\rho} - \boldsymbol{\rho}')\,, \tag{24}$$

where $s = E + i\epsilon$ is the complex spectral parameter.

Using field-theoretical techniques [64, 65, 70, 59] the configuration integral can be performed exactly, leading to an interacting field theory, which can be transformed to an effective field theory for a variable $Q(\mathbf{r}, s)$, which replaces the fluctuations $\Delta(\boldsymbol{\rho})$. A saddle-point approximation then leads to a mean-field equation for the saddle-point variable $Q_{\mathrm{saddle}}(s) = \Sigma(s)$ (self energy), which is obtained by minimizing the saddle-point action.

This equation is the self-consistent Born equation (SCBA), which may be obtained also from the lowest-order perturbation theory [71] and then replacing the non-interacting Green's function by the perturbed one. The averaged Green's function for the perturbed (disorder-affected) system is written in terms of a complex self-energy function $\Sigma(s)$ in the following way:

$$\begin{aligned} G(q,s) &= \int d\{\boldsymbol{\rho} - \boldsymbol{\rho}'\} e^{i\mathbf{q}[\boldsymbol{\rho}-\boldsymbol{\rho}']} \big\langle \mathsf{G}(\boldsymbol{\rho}, \boldsymbol{\rho}', \mathsf{s}) \big\rangle \\ &= \frac{1}{-s + q^2\big[1 - \Sigma(s)\big]} = \frac{1}{1-\Sigma(s)} \frac{1}{q^2 - k_\Sigma^2(s)} \qquad (25) \\ &\approx \frac{1}{1-\Sigma'(0)} \frac{1}{q^2 - k_\Sigma^2(s)} \qquad (26) \end{aligned}$$

where we have introduced an E dependent complex wave number $k_\Sigma(s) = k'_\Sigma(\mathsf{E}) + ik''_\Sigma(\mathsf{E})$, which obeys

$$k_\Sigma^2(s) = \frac{s}{1 - \Sigma(s)} \tag{27}$$

The SCBA self-consistent equation for $\Sigma(s)$ is

$$\Sigma(s) = \gamma \sum_{\mathbf{q}} q^2 G(q,s) = \gamma \sum_{\mathbf{q}} \frac{q^2}{-s + q^2\big(1 - \Sigma(s)\big)} = \frac{\gamma}{1-\Sigma(s)} \Big(1 + sG(s)\Big) \tag{28}$$

with the local Green's function

$$G(s) = \sum_{\mathbf{q}} G(q,s) = \frac{1}{1-\Sigma'} \underbrace{\frac{2}{q_c^2} \int_0^{q_c} q dq}_{\sum_q} \frac{1}{-k_\Sigma(s)^2 + q^2} = \frac{1}{1-\Sigma'} \frac{1}{q_c^2} \Big[\ln(q_c^2 - k_\Sigma^2) - \ln(-k_\Sigma^2) \Big]\,. \tag{29}$$

Here we introduced an upper cutoff $q_c \propto \ell_c^{-1}$, which terminates the spatial spectrum of the modulus fluctuations[2]. From the local Green's function we obtain the *spectral density* as

$$\rho(\mathsf{E}) = \mathrm{Im}\left\{\frac{1}{\pi}G(s)\right\} = \frac{1}{\pi}\frac{2}{q_c^2}\int_0^{q_c} dqqG''(q,\mathsf{E}) = \frac{1}{q_c^2(1-\Sigma')}\theta(q_c^2(1-\Sigma') - \mathsf{E}) \tag{30}$$

For $\mathsf{E} \ll q_c^2$ we have

$$\Sigma'(\mathsf{E}) \approx \Sigma'(0) = \frac{\gamma}{1-\Sigma'(0)} \tag{31}$$

which can be solved to give

$$\Sigma(0) = \frac{1}{2}\left(1 - \sqrt{1-4\gamma}\right) \overset{\gamma\ll 1}{\approx} \gamma \tag{32}$$

Making a variable change $v = q^2$ and neglecting the imaginary part of k_Σ^2 in the denominator, we obtain for the imaginary part of the self energy

$$\mathrm{Im}\Big\{\Sigma(s)\big[1-\Sigma(s)\big]\Big\} = \Sigma''(\mathsf{E})\big[1-2\Sigma'(\mathsf{E})\big] = \gamma\mathrm{Im}\left\{\frac{1}{q_c^2}\int dv\frac{v}{-k_\Sigma'^2+v}\right\} = \gamma\frac{\pi}{q_c^2}{k'_\sigma}^2(\mathsf{E})\,, \tag{33}$$

from which follows

$$\Sigma''(\mathsf{E}) = \gamma\mathsf{E}\frac{\pi}{q_c^2}\frac{1}{1-2\Sigma'(\mathsf{E})}\frac{1}{1-\Sigma'(\mathsf{E})} \overset{\gamma\ll 1}{\approx} \gamma\mathsf{E}\frac{\pi}{q_c^2} \tag{34}$$

We now want to relate $\Sigma''(\mathsf{E})$ to the mean-free path of the scattered waves. We may Fourier-transform the Green's function (24) into $\boldsymbol{\rho}$ space to obtain

$$G(\boldsymbol{\rho},s) = -\frac{1}{4(1-\Sigma')}H_0^{(1)}\big(k_\Sigma(s)\rho\big) \overset{\rho\gg k_\Sigma^{-1}}{\longrightarrow} -\frac{1}{4(1-\Sigma'}\sqrt{\frac{2}{\pi k_\Sigma(s)\rho}}\,e^{ik_\Sigma(s)\rho} \tag{35}$$

Here $H_0^{(1)}(z)$ is the Hankel function of first kind [74]. For large ρ the intensity is then given by

$$\big|G(\boldsymbol{\rho},s)\big|^2 = \frac{1}{8\pi k_\Sigma(s)\rho}e^{-\rho/\ell(\mathsf{E})} \tag{36}$$

with the mean-free path given by [**?**]

$$\frac{1}{\ell(\mathsf{E})} = 2k''(\mathsf{E}) = k'_\Sigma(\mathsf{E})\frac{\Sigma''(\mathsf{E})}{1-\Sigma'(\mathsf{E})} \propto \mathsf{E}^{3/2} \tag{37}$$

As stated above the spectral parameter E stands for the squared frequency ω^2 in a true two-dimensional classical-wave system. We therefore identify $\ell \propto \mathsf{E}^{-3/2}$ as the *Rayleigh law* for wave attenuation of the quasi two-dimensional waves. As in all other classical-wave systems [70] the disorder scattering for small frequencies vanishes due to the Rayleigh divergence. Therefore, as we shall see below, for $\mathsf{E} \to 0$ the disorder becomes irrelevant, and in this limits there is no scattering (and hence no localization). But this result is somewhat trivial, because a ray launched exactly parallel to the optical axis, and hence to the direction of the the microfibers, does not experience the disorder.

[2] We could have included correlations of the modulus fluctuations in our calculations [72, 73, 71]. Then the q integration in the resulting SCBA equation goes over the Fourier transform of the correlation function $K(q)$. The latter then terminates the fluctuation spectrum. So introducing the infrared cutoff q_c includes schematically this effect.

3.3.2 Diffusion of the wave intensity

The multiple scattering of waves in a turbid medium can be well described in terms of a random walk along the possible paths among the scattering centers [75]. The scattered intensity may be shown to obey a diffusion equation. Our object of interest is therefore the intensity propagator

$$\begin{aligned} P(\mathbf{q},p,\mathsf{E}) &= \frac{1}{(2\pi)^2}\int d^2\mathbf{k}\left\langle G\big(\mathbf{k}+\tfrac{1}{2}\mathbf{q},s_+ +\tfrac{1}{2}\omega\big)G\big(\mathbf{k}-\tfrac{1}{2}\mathbf{q},s_- -\tfrac{1}{2}\omega\big)\right\rangle \\ &= \int_{-\infty}^{\infty} d\boldsymbol{\rho}\int_0^{\infty} d\tau e^{-p\tau}e^{-i\boldsymbol{\rho}\mathbf{q}}P(\boldsymbol{\rho},\tau,\mathsf{E}) \end{aligned} \tag{38}$$

with $p \equiv -i\omega+\epsilon$, $\epsilon \to +0$. The second line defines $P(\mathbf{q},p,E)$ as the spatial Fourier transform and Laplace transform (with respect to τ) of the intensity propagator $P(\boldsymbol{\rho},\tau,\mathsf{E})$ in the $\boldsymbol{\rho}=(x,y)$ plane. For deriving the diffusion description it is assumed that after each scattering event the memory of the phase of the wave function is lost. $P(q,p,\mathsf{E})$ then obeys a diffusion equation with a E dependent modal "diffusivity"[3] $D(p,\mathsf{E})$:

$$\left(\frac{\partial}{\partial\tau}-\nabla^2_{\boldsymbol{\rho}}D_0(\mathsf{E})\right)P(\boldsymbol{\rho},\tau,\mathsf{E})=\delta(\boldsymbol{\rho})\delta(\tau) \qquad \Leftrightarrow \qquad P(\mathbf{q},p,\mathsf{E})=\frac{1}{p+q^2D_0(\mathsf{E})} \tag{39}$$

As a matter of fact, whithin the saddle-point approximation (SCBA) one is able to calculate the mean-field diffusion coefficient $D_0(\mathsf{E})$, which corresponds to the diffusion approximation. This diffusivity is the analogue to the electronic diffusivity $D_0=\sigma_0/\rho_F$, where σ_0 is the Drude conductivity and ρ_F the density of states at the Fermi level. D_0 is obtained by considering the Gaussian fluctuations of the field variable $Q(\boldsymbol{\rho},s)$ around $Q_{\mathrm{saddle}}(s)$ [64, 65, 70, 59**?**] and is given by

$$D_0(\mathsf{E})=\frac{\ell(\mathsf{E})k'_\Sigma(\mathsf{E})}{q_c^2\rho(\mathsf{E})} \tag{40}$$

This diffusivity may be related to a dimensionless modal conductivity g_0 by the Einstein relation

$$g_0=q_c^2\rho(\mathsf{E})D_0(\mathsf{E})=\ell(\mathsf{E})k_\Sigma(\mathsf{E})=\frac{D_0}{1-\Sigma'(0)}=\frac{1-\Sigma'(\mathsf{E})}{\Sigma''(\mathsf{E})}\overset{\gamma\ll 1}{\approx}\frac{q_c^2}{\pi}\frac{1}{\gamma\mathsf{E}} \tag{41}$$

We see that g_0 and D_0 in our model are equal to each other to within a factor of order unity. In two dimension the conductivity is also equal to the conductance. This quantity is relevant to the scaling approach of Anderson localization, which will be explained in the beginning of the next section. For $\mathsf{E}\to 0$ the conductance g_0 diverges due to the Rayleigh law [70].

3.4 Anderson localization

3.4.1 Wave interference and the scaling theory of Anderson localization

The diffusion approximation assumes that after each scattering event the phase memory is lost. However, if one follows the scattering amplitudes with phases kl_{ij}, (where l_{ij} is the distance between two adjacent scattering centers,) in a frozen medium, the phase memory is in principle not lost. This has dramatic consequences for recurrent partial paths, i.e. paths with closed loops: The phase of the recurrent path is exactly equal to that going in the reverse direction (see Fig. 9). This leads to destructive interference and therefore to a *decrease* of the diffusivity and, as we shall see, for d = 2 to a vanishing of the diffusivity.

[3] It is important to note that the "diffusivity" $D(p,\mathsf{E})$ is dimensionless, because the "frequency" $p=-i\omega+\epsilon$ has the dimension of an inverse squared length.

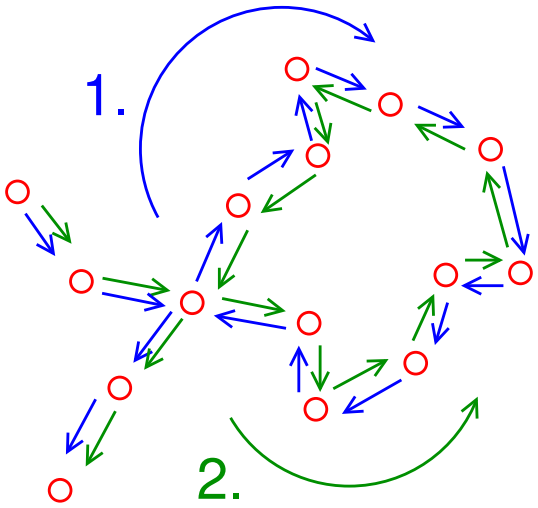

Figure 9. Visualization of two interfering scattering parths, one going clockwise along the loop, the other anticlockwise.

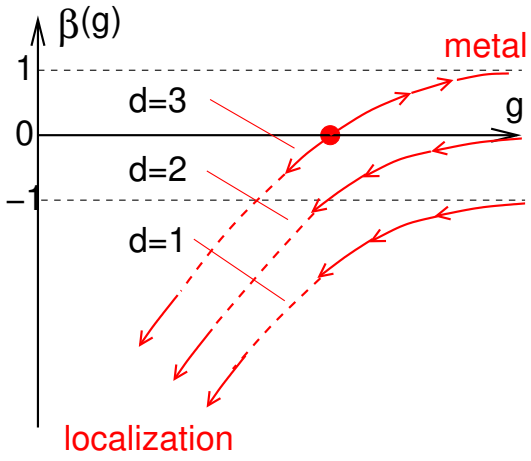

Figure 10. Sketch of the scaling function as anticipated by Abrahams, Anderson, Licciardello and Ramakrishnan [62].

For describing the interference mechanism Abrahams et al. [62] have proposed an ingenious scaling scenario. They consider the dependence of a dimensionless conductance g on the sample size L in d dimensions and make the Ansatz

$$g(L) \propto L^{\beta} \qquad \Leftrightarrow \qquad \beta = \frac{d \ln g}{d \ln L} \tag{42}$$

For $\beta > 0$ g scales towards infinity with increasing L, for $\beta < 0$ g scales towards zero. In the metallic regime ($g \to \infty$) the conductance should depend on the size L of a sample as $g(L) \propto \sigma L^{d-2}$, where σ is the conductivity, so that $\beta(g \to \infty) = d - 2$ (see Fig. 10). On the other hand, for localization ($g \to 0$) one expects $g(L) \propto e^{-L/\xi}$, where ξ is the localization length. This transforms to $\beta(g \to 0) \propto \ln g$. Abrahams et al. then assumed a smooth interpolation between the two limits to exist (see Fig. 10). By means of perturbation theory they further estimated the correction due to the interference terms to be negative and

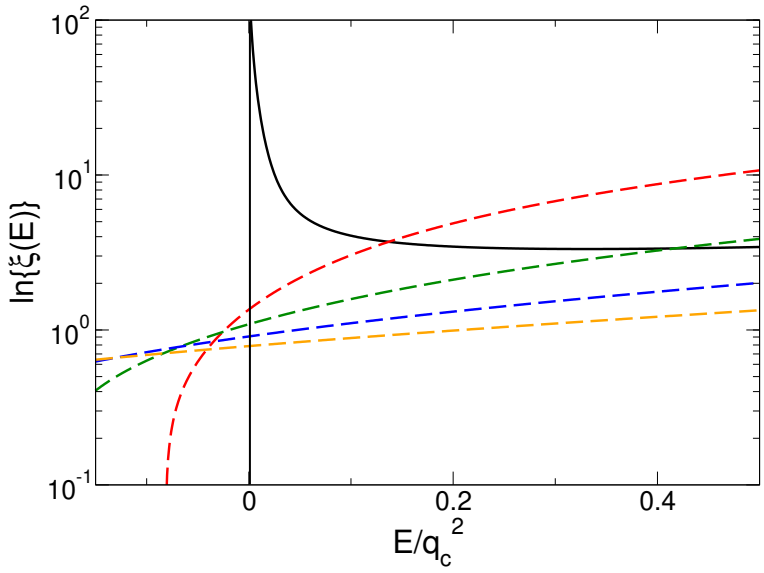

Figure 11. Logarithm of the localization length $\ln \xi(\mathsf{E}) \propto g_0(\mathsf{E})$ as a function of the spectral parameter $\mathsf{E} = k_0^2 \sin(\theta)^2$ Full line: MT calculation. Broken lines: PT calculation for several wavenumbers k_0.

proportional to $1/g$. Their final result for the scaling function is

$$\beta(g) = \frac{\partial \ln g}{\partial \ln L} = d - 2 - \frac{c}{g} \tag{43}$$

where c is of the order of 1. In 3 dimension the scaling with increasing size L depends on the initial value of the conductance, i.e. on the conductivity in diffusion approximation (Drude approximation for electrons). However, as can be seen from Fig. 10 in 2 and 1 dimension g scales always towards 0, i.e. for $L \to \infty$ there is always localization. The scaling function (43) is the same for the nonlinear sigma model for planar ferromagnetism, as noticed by Wegner [63]. Later a field-theoretical mapping from a stochastic Helmholtz equation to a generalized nonlinear sigma model was established and applied to the electronic Anderson problem [64, 65] as well as the PT description of the classical-wave problem [70, 1] and the MT description of acoustical [59] waves and light [50].

In two dimensions the scaling equation (43) is solved as

$$g(L) = -c \ln L/L_0 + g_0 \tag{44}$$

The localization length is given by the value L takes for $g_1 \approx 1$. The reference conductance g_0 is that in the diffusion approximation given by Eq. (41). For the reference length we take $L_0 = \frac{1}{q_c} e^{-1/c}$. Then we obtain the well-known formula for two dimension [76]:

$$\xi(\mathsf{E}) = \frac{1}{q_c} e^{g_0(\mathsf{E})/c} \tag{45}$$

In Fig. 12 we have plotted the localization length as a function of the spectral parameter using the SCBA for calculating g_0 [50]. We compare the result with the one obtained from the PT approach, in which the disorder potential explicitly depends on the wavenumber k_0 of the laser. We make the following observations;

- In the MT approach the localization length diverges for $\mathsf{E} \to 0$ (Rayleigh divergence). As mentioned above, this must be so, because a ray launched exactly in the direction of the optical axis does not explore the transverse disorder. On the other hand, this property is violated by the PT approach
- The MT theory gives a spectrum only for positive values of E. This is required for a spectrum of bosonic excitations. This stability requirement is violated by the PT approach

We already showed at the end of Section 2 that from our measurement of the average localization length of transverse-localized fibers we did not find any dependence on k_0. So both from the theoretical as well as the experimental standpoint the PT approach is invalid and should be abandoned.

3.4.2 Analytical description of the z dependence of the radius of the localized modes

The localization properties of the wave intensity can be efficiently be described by a *frequency-dependent* diffusivity $D(p, \mathsf{E})$. The generalized diffusion propagator then takes the form

$$P(\mathbf{q}, p, \mathsf{E}) = \frac{1}{p + q^2 D(p, \mathsf{E})} \tag{46}$$

An important quantity for describing the spread of the wave intensity in the (x, y) plane is the mean-square displacement

$$R^2(\tau, \mathsf{E}) = \int d^2\boldsymbol{\rho} \rho^2 P(\boldsymbol{\rho}, \tau, \mathsf{E}) = -\nabla^2_{\mathbf{q}} P(q, \tau, \mathsf{E})\Big|_{q=0}, \tag{47}$$

$\sqrt{R^2(\tau, \mathsf{E}_i)}$ is the radius of the mode E_i as a function of $\tau = z/2k_0$. For the Fourier transform we have

$$R^2(p) = -\nabla^2_{\mathbf{q}} P(q, \mathsf{E}, p)\Big|_{q=0} = \frac{4}{p^2} D(p, \mathsf{E}) \tag{48}$$

In the case of delocalization $\lim_{p\to 0} D(p, \mathsf{E})$ takes a real value $D(0, \mathsf{E})$. This implies that $\lim_{\tau\to\infty} R^2(\tau)$ increases linearly with τ as $R^2(\tau, \mathsf{E}) \propto D(0, \mathsf{E})\tau$. As we have stated above, this does not happen in two dimensions. Instead $\lim_{p\to 0} D(p, \mathsf{E}) = 0$ and $\lim_{\tau\to\infty} R^2(\tau) = const. = 4\xi^2(\mathsf{E})$, where $\xi(\mathsf{E})$ is the localization length. We may define a frequency-dependent squared localization length

$$\xi^2(p, \mathsf{E}) = \frac{1}{p} D(p, \mathsf{E}), \tag{49}$$

which obeys $\xi^2(p{=}0) = \xi^2(\mathsf{E})$. Its Laplace backtransform therefore obeys $\xi^2(\mathsf{E}) = \int_0^\infty \xi^2(\tau, \mathsf{E})$. For the mean-square displacement we have

$$R^2(p, \mathsf{E}) = 4\frac{1}{p}\xi^2(p, \mathsf{E}) \quad \Leftrightarrow \quad R^2(\tau, \mathsf{E}) = 4\int_0^\tau d\tau' \xi^2(\tau', \mathsf{E}) \tag{50}$$

According to the localization theory of Vollhardt and Wölfle [53, 66, 67, 57] in d dimensions the resistance increase due to the interference effect with respect to the diffusion-approximation resistance $1/D_0(\mathsf{E})$ is given by [53, 66, 67, 57]

$$\frac{1}{D(p, \mathsf{E})} - \frac{1}{D_0(\mathsf{E})} = \frac{c'}{D_0(\mathsf{E})} \int_0^{q_c} q^{d-1} dq \frac{1}{p + q^2 D(p, \mathsf{E})} \tag{51}$$

where c' is, again, a constant of order unity[4]. The term on the right-hand side is just the contribution due to the closed paths , which is proportional to $\lim_{\boldsymbol{\rho}\to 0} P(\rho, E, p)$ [77].

In $d = 2$ Eq. (51) can be re-written as

$$1 - \frac{D(p, \mathsf{E})}{D_0(\mathsf{E})} = \frac{c'}{D_0(\mathsf{E})} \int_0^{q_c} q dq \frac{1}{\frac{p}{D(p,\mathsf{E})} + q^2} = \frac{c'}{2D_0(\mathsf{E})} \ln\left(1 + q_c^2 \frac{D(p, \mathsf{E})}{p}\right) \tag{52}$$

For $p \to 0$ this equation has only a solution if $D(0, \mathsf{E}) = 0$, i.e. the system is localized. Replacing $\lim_{p\to 0} p/D(p, \mathsf{E})$ on the right-hand side of Eq. (52) by $\xi^2(\mathsf{E})$ and setting $D(E, p{=}0)$ = 0 on the left-hand side, we obtain

$$1 = \frac{c'}{2D_0(\mathsf{E})} \ln\left(1 + q_c^2 \xi_0^2(\mathsf{E})\right) \tag{53}$$

from which follows

$$\xi^2(\mathsf{E}) = \frac{1}{q_c^2}\left(\mathbf{e}^{\frac{2}{c'} D_0(\mathsf{E})} - 1\right) \approx \mathbf{e}^{\frac{2}{c'} D_0(\mathsf{E})} \tag{54}$$

Taking into account $D_0 = g_0[1 - \Sigma(0)]$ $\big($Eq. (41)$\big)$, we recover the scaling result (45) if we take $c' = c\big(1 - \Sigma(0)\big)$. It has been demonstrated in Ref. [67] that quite generally the scaling relation (43) can be derived in d dimensions from the self-consistent theory.

In order to evaluate $\xi^2(p, \mathsf{E})$ and $R^2(p, \mathsf{E})$ at finite p we represent $\xi(p, \mathsf{E})$ as

$$q_c^2 \xi^2(p, \mathsf{E}) \equiv \tilde{\xi}(p, \mathsf{E}) = \frac{q_c^2 D_0(\mathsf{E})}{p + \nu(p, \mathsf{E})} \equiv \frac{1}{\tilde{p} + \tilde{\nu}(p, \mathsf{E})} \tag{55}$$

where we introduced the dimensionless quantities $\tilde{p} = p/q_c^2 D_0(\mathsf{E})$ and $\tilde{\nu}(\mathsf{E}) = \nu(\mathsf{E})/q_c^2 D_0(\mathsf{E})$. The self-consistent equation (52) then takes the form

$$1 - \frac{D(p, \mathsf{E})}{D_0(\mathsf{E})} = \frac{\tilde{\nu}(p, \mathsf{E})}{\tilde{p} + \tilde{\nu}(p, \mathsf{E})} = \frac{1}{\tilde{g}_0(\mathsf{E})} \ln\left(1 + \frac{1}{\tilde{p} + \tilde{\nu}(p, \mathsf{E})}\right) \tag{56}$$

with $\tilde{g}_0(\mathsf{E}) = 2D_0(\mathsf{E})/c'$.

[4] In the original work of Vollhardt and Wölfle [53, 66, 67] the inverse mean free path ℓ^{-1} has been taken as ultraviolet cutoff. Both, because in our case $\ell(\mathsf{E})$ depends strongly on the spectral parameter E and for consistency reasons we use the correlation cutoff q_c as UV cutoff.

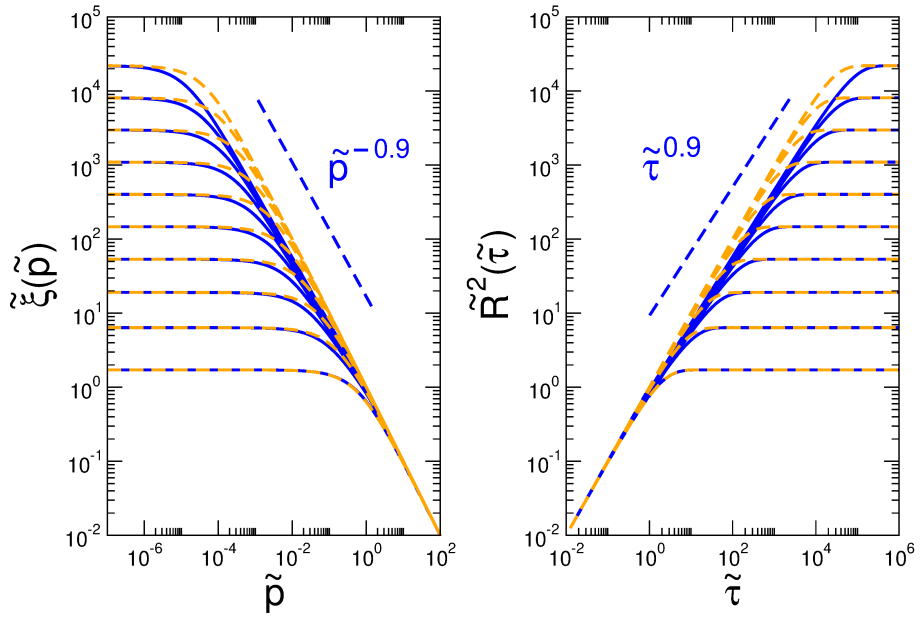

Figure 12. Left panel: The function $\chi(\tilde{p})$ evaluated by the self-consistent theory, Eq. (56) as a function of real $\tilde{p}$ (blue continuous curves), compared with the approximation (58), in which $\nu(p)$ has been replaced by $\nu(0,\mathsf{E}) = 1/\tilde{\xi}^2(E)$ (orange dashed curves). The values of $\tilde{g}_0$ are (from bottom to top) 1, 2, . . . , 10. Right panel: The corresponding functions $\tilde{R}^2(\tilde{\tau})$

We further introduce a dimensionless mean-square displacement

$$\tilde{R}^2(\tilde{\tau}) = \frac{1}{4} q_c^2 R^2(\tau) = \int_0^{\tilde{\tau}} d\tilde{\tau}' \tilde{\xi}(\tilde{\tau}') \tag{57}$$

with $\tilde{\tau} = \tau q_c^2 D_0(\mathsf{E})$.

In the left-hand panel of Fig. 12 we show the function $\tilde{\xi}(\tilde{p})$, Eq. (55), evaluated from the self-consistent equation (56), as a function of real $\tilde{p}$. We compare with an approximation introduced recently by the present authors [78] in a description of transverse Anderson localization of light in the potential-type formalism

$$\tilde{\xi}(\tilde{p}) \approx \frac{1}{\tilde{p} + 1/\tilde{\xi}^2(\mathsf{E})} \quad \Leftrightarrow \quad \tilde{R}^2(\tilde{\tau}) = \tilde{\xi}^2(\mathsf{E}) \left(1 - e^{-\tilde{\tau}/\tilde{\xi}^2(\mathsf{E})}\right) \tag{58}$$

with $\tilde{\xi}(\mathsf{E}) = e^{\tilde{g}_0(\mathsf{E})} - 1$. We see that for small $\tilde{g}_0(\mathsf{E})$ this approximation works well. However for large $g(\mathsf{E})$, i.e. for small γ and/or E there is a region with a fractal frequency dependence $\tilde{\xi}(\tilde{p}) \propto \tilde{p}^{-0.9}$. Accordingly in the corresponding $\tilde{\tau}$ regime the squared mode radius $\tilde{R}^2(\tilde{\tau})$ (right-hand panel of Fig. 12) does not increase linearly but sublinearly arrording to $\tilde{R}^2(\tilde{\tau}) \propto \tilde{\tau}^{0.9}$. Obviously in the weakly localized regime, where the localization length might exceed the sample dimensions, the mode still does not behave like a delocalized mode, for which $R^2(\tau)$ would increase linearly. Instead the weakly localized modes exhibit *anomalous diffusion* with a fractal increase of the mean-square displacement.

3.5 Discussion

In this section we have presented a comprehensive theory of transverse Anderson localization of light. We started to derive the appropriate stochastic Helmholtz equation for electromagnetic waves with spatially fluctuating permittivity. We have shown, that the potential-type approach, which is analogous to the

Schrödinger equation for an electron in a random potential with the potential depending on the spectral parameter E, relies on an approximation, which is only applicable to very weak disorder, and, for transverse disorder leads to a wavelength dependence of the localization length. Such a depencence is not observed. In the newly introduced modulus-type approach, which is exact, such a dependence is not predicted, in agreement to our experiments.

Whithin the modulus-type approach the localization length, i.e. the radius of the transmitted modes, diverges as the spectral parameter (which is proportional to the square of the azimuthal angle between the direction of the incident radiation and the optical angle) vanishes. This must be so, because a ray in the direction of the optical axis does not experience transverse disorder. The potential-type approach, however, implies a finite mean-free path at zero spectral parameter, and the predicted spectrum penetrates into the negative range of E, rendering the predicted specrum unstable.

Using the self-consistent localization theory of Vollhardt and Wölfle we presented an analytic theory for the development of the width of the mean radius of the localized modes as a function of z. We showed that in the weakly localized regime (small disorder variance and/or small spectral parameter) the ray does not spread diffusively but exhibits anomalous diffusion.

At the end of this section we would like to comment on the possibility of observing localization of light in three-dimensional systems. As mentioned in the introduction, despite of intensive efforts, this has not been observed until now. We emphasized that the modulus-type theory is analogous to sound waves in solids with spatially fluctuating shear modulus. There it is known that localized states exist at the upper band edge, which in solids is the Debye frequency. In turbid media the analogue of the upper band edge is the inverse of the correlation length of the disorder fluctuations. So if it would be possible to prepare materials with spatial fluctuations of the dielectric modulus, which have a correlation length of the order of the light wavelength, we expect chances for observing 3-dimensional Anderson localization.

4 NON-CLASSICAL ANDERSON LOCALIZATION OF LIGHT

According to the seminal studies by Anderson regarding single-particle evolution in lattices, the disorder in the system leads to localization of the wave-function. As we have illustrated in the first sections, such a phenomenon is well explained by quantum mechanics in the case of electrons and by classical electrodynamics in the case of light in the classical limit, i.e. no quantum effects involved. In particular, localization is the result of constructive and destructive interference among the multiple paths of the particle. Being an explicit example of the wave-like behaviour of quantum particles, the observation of AL in single-photon states does not display any substantial difference with respect to the experiments carried out with classical light. However, single-photons are one of the most promising candidates for quantum information processing in the context of computation, simulation, and cryptography [79]. In this framework, AL has been extensively investigated in photonic quantum walks [80, 81, 82, 83]. The latter are versatile platforms for several tasks [84, 85], including simulation of quantum transport effects such as the AL. Furthermore, localized single-photons have been used as a resource to realize quantum cryptography protocols [86, 87]. The investigation of AL at the single-particle level reveals distinctive features when particle-particle interference is taken into accounts [88, 89]. This occurs when more than one particle evolves in the disordered lattice. In this case, other quantum properties of the system, such as particle indistinguishability and statistics, play a crucial role in the spatial distribution of the multi-photon wave-function.

This section regarding quantum AL is organized as follows. First, we introduce the quantum walks model and present single-photon experiments in the context of AL. We further provide practical applications of localized single-photon states in quantum cryptography protocols. Second, we illustrate two-photon quantum walks experiments and the effect of particle statistics in the localization.

4.1 Single-photon localization

4.1.1 Quantum walks

Quantum walks (QW) was first formulated as a generalization of classical random walks (RW) [90]. In the discrete-time evolution, the walker is replaced by a quantum particle which lives in an Hilbert space of d levels corresponding to the position in the lattice. In the RW the walkers goes forward or inward according to the result of a coin toss. In the quantum case, the coin toss is a unitary operator that manipulates an additional two-dimensional degree of freedom embedded in the walker. Then the state of a quantum walker is described by the eigenstates of the position operator $w = \{|d\rangle\}$ and by the coin basis $c = \{|\uparrow\rangle, |\downarrow\rangle\}$. The evolution is regulated by two operators, the *coin* $\hat{\mathcal{C}}$ that performs rotations in the coin subspace and the *shift* $\hat{\mathcal{S}}$. The latter moves the position of the walkers conditionally to the coin state c according to the following expression:

$$\hat{\mathcal{S}} = \sum_d |d+1\rangle\langle d| \otimes |\uparrow\rangle\langle\uparrow| + |d-1\rangle\langle d| \otimes |\downarrow\rangle\langle\downarrow| \tag{59}$$

The evolution operator in the discrete-time scenario is the combination of the coin and shift action, namely $U_n = (\hat{\mathcal{S}} \cdot (\hat{\mathcal{C}} \otimes \hat{\mathbb{I}}_w))^n$, where n is the number of single time-step evolution and $\hat{\mathbb{I}}_w$ is the identity operator in the walker's position space. It is possible to retrieve the evolution operator through the Hamiltonian $\mathcal{H}$ of the system describing a particle evolving in a lattice as $U(t) = e^{-i\mathcal{H}t}$. In this scenario it is straightforward to translate the above description to the continuous-time case. The main feature of the QW with respect to a RW with an unbiased coin is the distribution of the walker for $t \to \infty$. Such distribution depends by the initial state of the particle and the walker tends to spread towards the far ends of the lattice. This

is in contrast to the typical diffusive behaviours of a RW. This discrepancy is due to the superposition principle in quantum mechanics that gives rise to the interference effects typical of waves. The formulation of QWs is very general and feasible for different applications and experimental implementations in the quantum information and quantum computation fields [91, 92, 84]. In particular, the formulation of QWs is very suitable for realization in photonic platforms [93]. In the various experiments of photonic QWs, the dynamic of the walker has been encoded in the degree of freedoms of single photon states, such as the polarization for the coin subspace and, for the walker's position, the optical path in bulk [94, 95] and integrated interferometer [96, 97, 98, 99, 100, 101], the time arrival to the detector [102], the modes supported by a multi-mode fiber [103], the angular [104, 105, 106] and the transverse momentum [107].

The QWs evolution operator can be modified for different tasks. For examples, the QWs paradigm has been exploited to observe topological-protected states [94, 108], to simulate system with non-trivial topology [105, 107] and to engineer high-dimensional quantum states [106]. For what concerns AL in discrete-time QWs, single-photon localization has been investigated by introducing site-dependent disorder in the QW evolution. Such condition is achieved implementing site-dependent coin operators. One example is the coin in the form

$$\hat{\mathcal{C}}_d = \frac{1}{\sqrt{2}} \begin{pmatrix} e^{i\phi_d^{\uparrow}} & 0 \\ 0 & e^{i\phi_d^{\downarrow}} \end{pmatrix} \cdot \begin{pmatrix} 1 & 1 \\ 1 & -1 \end{pmatrix}, \tag{60}$$

where random extracted phase-shifts $\phi_d^{\uparrow(\downarrow)}$ operates locally on the site d thus breaking the transnational symmetry of the systems. In Ref. [80] the authors present a discrete-time QWs encoded in the time arrival and polarization of single-photon states. The apparatus comprises two loops of different lengths. At each step the photons generated by a single-photon source choose the shortest or the longest path according to the polarization state that represents the coin space. The position of the particle is encrypted in time. The coin operators in the expression (60) were manipulated to reproduce (1) the ballistic spread of the quantum walker by fixing $\phi_d^{\uparrow(\downarrow)} = 0$, (2) AL localization with random extracted phase-shift and (3) the diffusion regime that resembles the behaviour of a classical random walker. This last condition is the result of a dephasing between the two polarization in (60) larger than the coherence time of the single-photon packets, that destroys the interference among the paths. This experiment was one of the first proof of AL at the single-photon level. Another example in this direction is Ref. [81]. Here the discrete-time QW was realized through a integrated optical circuit composed by a network of beam-splitter and phase-shifts [109, 110]. Single-photon localization was observed in the output modes of the optical circuit.

Further examples of single-photon localization regards continuous-time QWs. They are typically realized exploiting continuous-coupling among wave-guide arranged in a lattice in photonic chips. In this scenario, the time coordinate is replaced by the distance z covered during the propagation in the waveguides. The single-photon wave-function is given by the equation [111]:

$$-i\frac{\partial \psi_d}{\partial z} = c_{d,d}\psi_d + c_{d,d-1}\psi_{d-1} + c_{d+1,d}\psi_{d+1}, \tag{61}$$

where ψ_d is the single-photon amplitude in the site d and the coefficients c_{ij} are the couplings among the modes of the lattice. The length of the device and the couplings coefficients can be engineered to observe AL, as shown in the single-photon experiments in Refs. [82, 83].

In all the mentioned quantum experiments it is worth noting that the localized single-photon distribution has the same properties of the localized distribution of classical light described in section 2-3. The interest

in quantum localization is not restricted only to the pure observation of localized state. In the following section we illustrate an application of localized single-photon in quantum cryptography.

4.2 Quantum cryptography through localized single-photon states

Quantum computing could undermine the security of some of the current cryptographic protocol. An example is given by the RSA protocol whose security is based on the hardness for a classical computer to find prime-factors of large integer number, while a quantum computer solves the same problem in polynomial time [112]. This motivates the need of a different approach to produce more secure cryptographic procedure. Quantum cryptography is the field of quantum information that has the aim to formulate secure protocol based on the rules of quantum mechanics. In the quantum protocol BB84, two agents, Alice and Bob, exchange a stream of *qubits*, i.e. quantum states that lives in a two-dimensional Hilbert space. Alice randomly chooses to prepare the state according to two possible basis $\{|\uparrow\rangle, |\downarrow\rangle\}$ and $\{|+\rangle, |-\rangle\}$, where $|\pm\rangle = \frac{1}{\sqrt{2}}(|\uparrow\rangle \pm |\downarrow\rangle)$. Bob receives the signal and decides randomly in which basis measuring the qubits. He extracts a stream of bits corresponding to 0 when he measures $\uparrow$ $(+)$ and to 1 when he measures $\downarrow$ $(-)$. Then, Alice and Bob's streams of bits could not correspond when Bob measures in a basis different from the Alice's choice. The two agents compare part of their bit strings and, according to the resulting bits error rate, they can detect an eventual eavesdropper attack and extract a secure key [113]. Variants of this protocols exploits entangled states or high-dimensional states instead of qubits. The latter are a generalization of qubits and describe a particle living in a d-dimensional space. The so called *qudits* provide advantages in the amount of the information storage in the state send to the receiver, and security [114].

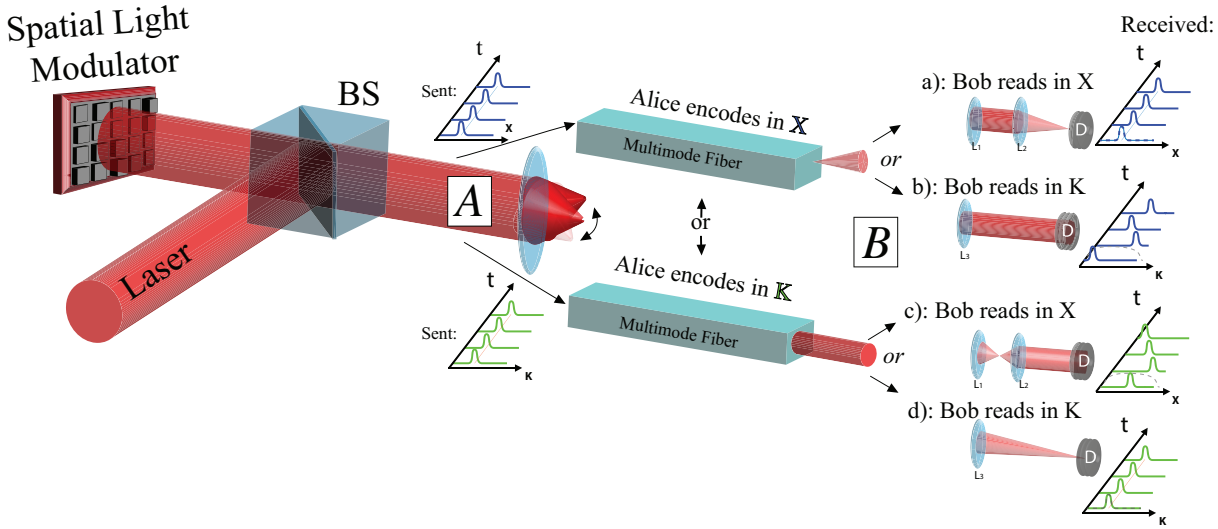

Figure 13. Experimental apparatus for quantum cryptography using single-photon localized states. Alice encodes her qudits by preparing single-photon states via a spatial light modulator. She chooses between two basis, namely (K) the eigenstates of the multimode fiber that localize after the propagation, and (X) the states that spread after the fiber. Bob measures in the K basis or in the X basis inserting one or two lens before the detection stage. After the comparison between the basis choices by Alice and Bob, they can extract a secure key.

Single-photon localized states are examples of qubits, where the d-levels correspond to the positions assumed by the photons. In Ref. [86] the authors implement a BB84-inspired protocol using localized states generated by disordered optical fiber. The experimental setup is similar to the one showed in Fig. 13.

Alice modulates the single photons obtained by an attenuated laser with a spatial light modulator. In this way she can choose to send states that localize after propagation in the fiber in either momentum or position at the fiber's output tip. Bob chooses the basis of the measurement by placing or removing a lens before the single-photon detector. This implementation of the BB84 exploits the duality between the real space and the Fourier space of the lens: a state localized in the first space is indeterminate in the other one and vice-versa. The authors prove the feasibility of the protocol using localized single-photon wave-function even in the experimental conditions. A recent work [87] exploits a similar setup for performing a slight different cryptografic protocol. In this experiment the information about the basis chosen by Alice is not shared publicly after the communication between the agents. Alice codifies her message and the basis in two different photons that are send at different random time. At the end of the protocol Alice and Bob compare the measurements about some random pair of photons and then, they are able to extract a secure key. This protocol offers advantages in terms of sensitivity to noise and resilience to "photon number splitting" eavesdropper attack.

4.3 Multi-photon localization

Single-photon localized states do not add any further insight into AL with respect to experiments based on waves interference. Nevertheless, the proper description of quantum light is within the framework of second quantization. This representation is necessary for describing many-particle evolution. The electromagnetic field can be expressed by the boson annihilation $\hat{a}$ and creation operators $\hat{a}^\dagger$, i.e. the operators that destroy or create exactly one photon in a given mode [115]. Such description considers the particle statistics and, consequently, explains the quantum interference effects due to particles' indistinguishability. This change of paradigm in the state's description consists basically in expressing the same state in terms of occupation numbers of the field modes. The systems is then individuated by the evolution operator acting to the creation and annihilation operators. In the case of QWs, that, as we have seen in the previous section, corresponds to a linear transformation among modes of a given degree of freedom, the single creation operators representing one photon in the mode i will be

$$\hat{b}_i^\dagger = \sum_j U_{ij} \hat{a}_j^\dagger \tag{62}$$

where U_{ij} are the element of the QW evolution operator in the occupation number representation. One of the most famous example of two-photon interference, the Hong-Ou Mandel (HOM) experiment [116] is explained by the latter formulation. Here two indistinguishable photons entering in a beam-splitter from different ports come out always together in the same output port. This phenomenon is a first example of the role of particle indistinguishability in the evolution of multi-photon states.

Two-photon interference has been investigated in the regime of AL. The main result that emerges from these studies is that the way in which the system approaches localization strongly depends on its initial state. In Fig. 14 we report numerical simulations illustrating the two-photon state localization investigated in the theoretical [88, 117, 89] and the experimental works [81, 82, 83] carried out in this topic. The first row (Fig. 14 a-d) report the two-photon distribution $G(x_1, x_2)$ defined as the probability to detect one photon in the position x_1 and the other in x_2, averaged over different disorder configurations, i.e

$$G(x_1, x_2) = \langle\langle |\langle 0|\hat{a}_{x_1}\hat{a}_{x_2}|\psi\rangle|^2 \rangle\rangle = \langle\langle |U_{x_1,0}U_{x_2,1} + U_{x_2,0}U_{x_1,1}|^2 \rangle\rangle, \tag{63}$$

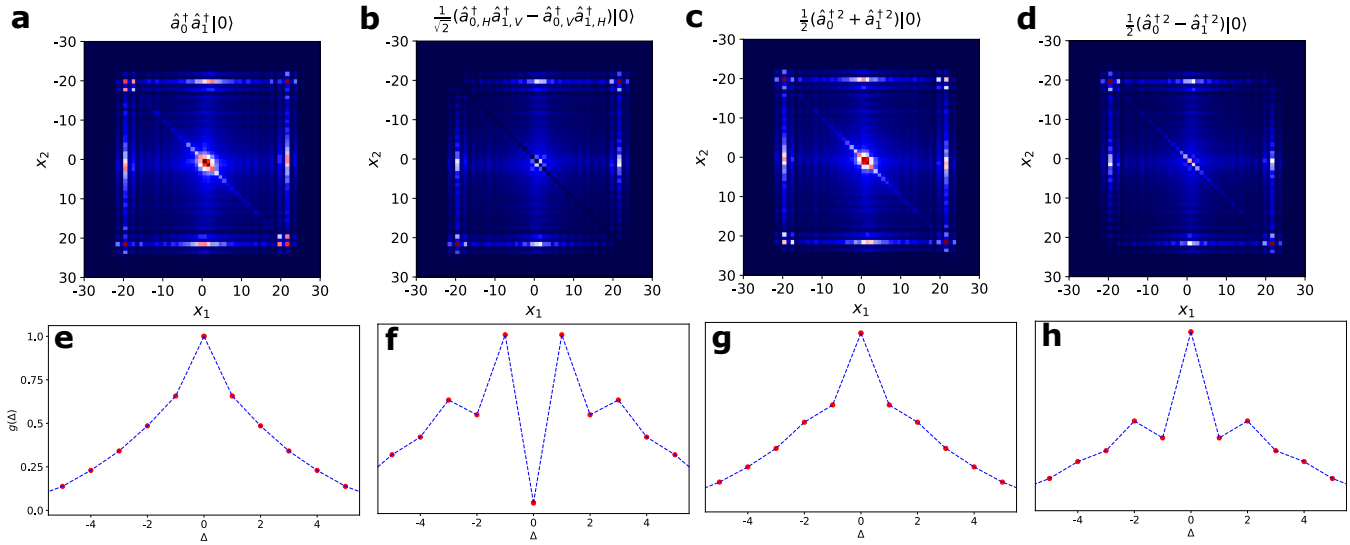

Figure 14. Two-photon quantum localization. **a-d** Correlations functions $G(x_1, x_2)$ of two-photon wave function in a one-dimensional Anderson lattice. The four scenarios report the distributions for different input states in an intermediate time evolution, where the two photons have the same chance to be localized or to spread balistically. a) photons are prepared in a separable state in which they occupy two adjacent sites. b) Entangled state in the polarization degree of freedom (H: horizontal polarization, V: vertical polarization) that is anti-symmetric under with respect to the exchange of the particles paths. Such state mimics the fermions statistics. Indeed, according to the Pauli exclusion principle, the probability to detect the two photons in the same site is zero. c-d) Entangled states in the occupation number of two sites. The distribution changes depending by the sign in the superposition. e-f) The function $g(\Delta)$ calculated in the localization area, i.e $x_1, x_2 \in [-4, 4]$ and $x_1 - x_2 = \Delta$ for the four initial states.

where $\langle\langle \cdot \rangle\rangle$ is the average over the disorder, the bra $\langle 0|\hat{a}_{x_1}\hat{a}_{x_2}$ is the projection on the state with the photons in the positions x_1 and x_2 respectively and the last terms expressing the probability through the matrix U of eq. (62). The distributions reported in the figure illustrate the state of the system after an intermediate time evolution. In such condition the single-photon wave-function still preserves the ballistic spread typical in the QW, while it is starting to localize. In the second row (Fig. 14e-h) we show the function $g(\Delta) = \sum_{x_1 - x_2 = \Delta} G(x_1, x_2)$ in the region of localization. All the quantities are normalized to the maximum and averaged among 1000 configurations of disorder. Figs. 14a-b and 14e-f compare the two functions G and g for the evolution of the initial states $\hat{a}_0^\dagger \hat{a}_1^\dagger |0\rangle$ and $\frac{1}{\sqrt{2}}(\hat{a}_{0,H}^\dagger \hat{a}_{1,V}^\dagger - \hat{a}_{1,H}^\dagger \hat{a}_{0,V}^\dagger)|0\rangle$. These states correspond to two photons created in the site 0 and 1 with different symmetries respect to the exchanging operations between the two particles. The first one reproduces the evolution of two non-interacting bosons. Here, we observe the typical tendency of bosons to assume the same states just mentioned in the description of HOM experiment, i.e to find the two photons in the same position with high probability. In contrast, the second state is anti-symmetric under exchanging of the two particles and presents the opposite behaviour. The probability to find the photons in the same site is zero. These states simulate *de facto* fermion statistics and the Pauli exclusion principle. To reproduce an anti-symmetric state it is necessary to exploit an additional degree of freedom, in this case the polarization. The boson and fermion statistics in AL has been observed experimentally for the first time in Ref. [81] by exploiting polarization entangled states and an integrated photonic chip. Here a single-photon source based on parametric down conversion from a nonlinear crystal generates a pair of entangled states in polarization such as the state investigated in Fig. 14b and f. The state evolves in a discrete QW platform realized in an integrated device that comprises a network of beam-splitter and phase-shifts (see section 4.1). The coin operators in the form of eq. (60) are sampled properly to observe the AL. The second type of states investigated in literature are

illustrated in Fig 14c-d and g-h. These states are entangled in the occupation number of the sites 0 and 1. The output distribution depends on the sign in the superpositions of the contributions $\hat{a}_0^{\dagger 2}$ and $\hat{a}_1^{\dagger 2}$, that create two photons in the respective modes. Such entangled states in the context of AL were investigated for the first time in [82] and then in [83]. The pair of entangled photons are generated via parametric down conversion. These photons are strongly correlated in the momentum space. Such correlations are transferred among the position of the QW's lattice by means of a lens system. In this way the photons are coupled in the waveguides of the integrated device implementing the QWs. The two experiments with such entangled states have been performed exploiting continuous-time QW by random couplings among the waveguides arranged in a lattice (see section 4.1). In particular, in the most recent experiment (Ref. [83]) the authors report the results averaged over different configurations of random couplings thus representing one of the most exhaustive experiment on two-photon AL localization.

4.4 Discussion

In this section we have illustrated the Anderson localization (AL) in the context of quantum light, presenting the most relevant results for what concerns the experimental realizations and applications. We have first formulated AL in the context quantum walks (QW). We have then described the use of localized states in quantum cryptography. In the end we have illustrated the problem of localization in quantum optics, by considering multi-photon states. Up-to-date the investigation of multi-photon AL localization was confined to the two-photon case. The reasons are various. It is still debated in the literature whether the results reported in the quantum experiments can be reproduced by classical light, i.e by wave interference. For instance, in Ref. [117] it was shown that some features of the distribution reported in Fig.14 could be observed with a laser propagating in a circuit engineered with a proper disorder. Other concerns regard the intrinsic hardness to simulate the evolution of non-interacting bosons such as photons scattered by a random networks [118]. This prevents finding an analytical solution for the systems with a large number of photons. All these considerations explain why the present investigations about quantum AL were basically carried out from a phenomenological perspective. This motivates further studies to provide a more rigorous framework for quantum AL.

REFERENCES

[1] John S. Electromagnetic absorption in a disordered medium near a photon mobility edge. *Phys. Rev. Lett.* **53** (1984) 2169–2172. doi:10.1103/PhysRevLett.53.2169.

[2] Anderson PW. The question of classical localization: A theory of white paint? *Philosophical Magazine Part B* **52** (1985) 505–509.

[3] Van Albada MP, Lagendijk A. Observation of weak localization of light in a random medium. *Physical review letters* **55** (1985) 2692.

[4] Wolf PE, Maret G. Weak localization and coherent backscattering of photons in disordered media. *Physical review letters* **55** (1985) 2696.

[5] Akkermans E, Wolf PE, Maynard R. Coherent backscattering of light by disordered media: Analysis of the peak line shape. *Phys. Rev. Lett.* **56** (1986) 1471–1474. doi:10.1103/PhysRevLett.56.1471.

[6] Wiersma DS, Bartolini P, Lagendijk A, Righini R. Localization of light in a disordered medium. *Nature* **390** (1997) 671–673.

[7] Störzer M, Gross P, Aegerter CM, Maret G. *Phys. Rev. Lett.* **96** (2006) 063904.

[8] Sperling T, Buehrer W, Aegerter C, Maret G. Direct determination of the transition to localization of light in three dimensions. *Nature Photonics* **7** (2012) 48.

[9] Scheffold F, Lenke R, Tweer R, Maret G. Localization or classical diffusion of light? *Nature* **398** (1999) 206–207.
[10] Sperling T, Schertel L, Ackermann M, Aubry GJ, Aegerter CM, Maret G. Can 3d light localization be reached in 'white paint' ? *New J. Physics* **18** (2016) 013039.
[11] Skipetrov SE, Page JH. Red light for Anderson localization. *New J. Physics* **18** (2016) 021001.
[12] Skipetrov SE, Sokolov IM. Absence of anderson localization of light in a random ensemble of point scatterers. *Physical review letters* **112** (2014) 023905.
[13] Abdullaev SS, Abdullaev FK. On light propagation in a system of tunnelcoupled waveguides. *Izv. Vuz. Radiofiz.* **23** (1980) 766.
[14] De Raedt H, Lagendijk A, de Vries P. Transverse localization of light. *Physical review letters* **62** (1989) 47.
[15] Born M, Wolf E. *Principles of optics: electromagnetic theory of propagation, interference and diffraction of light* (Elsevier) (2013).
[16] Pritchett TM, Trubatch AD. *Am. J. Phys.* **72** (2004) 1026.
[17] Anderson PW. Absence of diffusion in certain random lattices. *Phys. Rev.* **109** (1958) 1492.
[18] Schwartz T, Bartal G, Fishman S, Segev M. Transport and Anderson localization in disordered two-dimensional photonic lattices. *Nature* **446** (2007) 52–55.
[19] Efremidis NK, Sears S, Christodoulides DN, Fleischer JW, Segev M. Discrete solitons in photorefractive optically induced photonic lattices. *Physical Review E* **66** (2002) 046602.
[20] Karbasi S, Mirr CR, Yarandi PG, Frazier RJ, Koch KW, Mafi A. Observation of transverse anderson localization in an optical fiber. *Optics letters* **37** (2012) 2304–2306.
[21] Karbasi S, Hawkins T, Ballato J, Koch KW, Mafi A. Transverse Anderson localization in a disordered glass optical fiber. *Opt. Mater. Express* **2** (2012) 1496–1503.
[22] Chen X, Reichenbach KL, Xu C. Experimental and theoretical analysis of core-to-core coupling on fiber bundle imaging. *Optics express* **16** (2008) 21598–21607.
[23] Karbasi S, Frazier RJ, Koch KW, Hawkins T, Ballato J, Mafi A. Image transport through a disordered optical fibre mediated by transverse anderson localization. *Nature communications* **5** (2014) 1–9.
[24] Leonetti M, Karbasi S, Mafi A, Conti C. Observation of migrating transverse anderson localizations of light in nonlocal media. *Physical Review Letters* **112** (2014) 193902.
[25] Lahini Y, Avidan A, Pozzi F, Sorel M, Morandotti R, Christodoulides DN, et al. Anderson localization and nonlinearity in one-dimensional disordered photonic lattices. *Phys. Rev. Lett.* **100** (2008) 013906. doi:10.1103/PhysRevLett.100.013906.
[26] Sapienza L, Thyrrestrup H, Stobbe S, Garcia PD, Smolka S, Lodahl P. Cavity quantum electrodynamics with anderson-localized modes. *Science* **327** (2010) 1352–1355.
[27] Leonetti M, Karbasi S, Mafi A, Conti C. Experimental observation of disorder induced self-focusing in optical fibers. *Applied Physics Letters* **105** (2014) 171102.
[28] Snyder AW, Mitchell DJ. Accessible solitons. *Science* **276** (1997) 1538–1541.
[29] Conti C. Complex light: Dynamic phase transitions of a light beam in a nonlinear nonlocal disordered medium. *Phys. Rev. E* **72** (2005) 066620. doi:10.1103/PhysRevE.72.066620.
[30] Abrahams E. *50 Years of Anderson Localization* (WORLD SCIENTIFIC) (2010). doi:10.1142/7663.
[31] Ruocco G, Abaie B, Schirmacher W, Mafi A, Leonetti M. Disorder-induced single-mode transmission. *Nature communications* **8** (2017) 1–6.
[32] Lee PA, Ramakrishnan TV. Disordered electronic systems. *Rev. Mod. Phys.* **57** (1985) 287.
[33] Vynck K, Burresi M, Riboli F, Wiersma DS. Photon management in two-dimensional disordered media. *Nature materials* **11** (2012) 1017–1022.

[34] Liu J, Garcia P, Ek S, Gregersen N, Suhr T, Schubert M, et al. Random nanolasing in the anderson localized regime. *Nature Nanotechnology* **9** (2014) 285–289.

[35] Abaie B, Mobini E, Karbasi S, Hawkins T, Ballato J, Mafi A. Random lasing in an anderson localizing optical fiber. *Light: Science & Applications* **6** (2017) e17041–e17041.

[36] Mafi A. Transverse anderson localization of light: a tutorial. *Advances in Optics and Photonics* **7** (2015) 459–515.

[37] Bertolotti J. Designing disorder. *Nature Photonics* **12** (2018) 59–60.

[38] Zhou W, Tong Y, Sun X, Tsang HK. Hyperuniform disordered photonic bandgap polarizers. *Journal of Applied Physics* **126** (2019) 113106.

[39] Milošević MM, Man W, Nahal G, Steinhardt PJ, Torquato S, Chaikin PM, et al. Hyperuniform disordered waveguides and devices for near infrared silicon photonics. *Scientific reports* **9** (2019) 1–11.

[40] Pratesi F, Burresi M, Riboli F, Vynck K, Wiersma DS. Disordered photonic structures for light harvesting in solar cells. *Optics express* **21** (2013) A460–A468.

[41] Aubry GJ, Froufe-Pérez LS, Kuhl U, Legrand O, Scheffold F, Mortessagne F. Experimental tuning of transport regimes in hyperuniform disordered photonic materials. *Phys. Rev. Lett.* **125** (2020) 127402. doi:10.1103/PhysRevLett.125.127402.

[42] Gianfrate A, Dominici L, Ballarini D, Sanvitto D, Leonetti M. Transverse localization of light in laser written designed disorder. *Applied Physics Letters* **116** (2020) 071101.

[43] Gattass RR, Mazur E. Femtosecond laser micromachining in transparent materials. *Nature photonics* **2** (2008) 219–225.

[44] Martin L, Di Giuseppe G, Perez-Leija A, Keil R, Dreisow F, Heinrich M, et al. Anderson localization in optical waveguide arrays with off-diagonal coupling disorder. *Optics express* **19** (2011) 13636–13646.

[45] Stützer S, Kartashov YV, Vysloukh VA, Tünnermann A, Nolte S, Lewenstein M, et al. Anderson cross-localization. *Optics letters* **37** (2012) 1715–1717.

[46] Naether U, Meyer JM, Stützer S, Tünnermann A, Nolte S, Molina M, et al. Anderson localization in a periodic photonic lattice with a disordered boundary. *Optics letters* **37** (2012) 485–487.

[47] Naether U, Kartashov Y, Vysloukh VA, Nolte S, Tünnermann A, Torner L, et al. Observation of the gradual transition from one-dimensional to two-dimensional anderson localization. *Optics letters* **37** (2012) 593–595.

[48] Vicencio RA, Cantillano C, Morales-Inostroza L, Real B, Mejía-Cortés C, Weimann S, et al. Observation of localized states in lieb photonic lattices. *Physical review letters* **114** (2015) 245503.

[49] Stützer S, Plotnik Y, Lumer Y, Titum P, Lindner NH, Segev M, et al. Photonic topological anderson insulators. *Nature* **560** (2018) 461–465.

[50] Schirmacher W, Abaie B, Mafi A, Ruocco G, Leonetti M. What is the right theory for anderson localization of light? an experimental test. *Phys. Rev. Lett.* **120** (2018) 067401.

[51] Karbasi S, Mirr CR, Yarandi PG, Frazier RJ, Koch KW, Mafi A. Observation of transverse Anderson localization in an optical fiber. *Opt. Lett.* **37** (2012) 2304–2306.

[52] Karbasi S, Mirr CR, Frazier RJ, Yarandi PG, Koch KW, Mafi A. Detailed investigation of the impact of the fiber design parameters on the transverse Anderson localization of light in disordered optical fibers. *Opt. Express* **20** (2012) 18692–18706.

[53] Vollhardt D, Wölfle P. Anderson localization in $d \leq 2$ dimensions: A self-consistent diagrammatic theory. *Physical Review Letters* **45** (1980) 842.

[54] John S. Strong localization of photons in certain disordered dielectric superlattices. *Phys. Rev. Lett.* **58** (1987) 2486–2489.
[55] Kroha J, Soukoulis CM, Wölfle P. Localization of classical waves in a random medium: A self-consistent theory. *Phys. Rev. B* **47** (1993) 11093–11096.
[56] Sheng P. *Introduction to Wave Scattering, Localization and Mesoscopic Phenomena* (Heidelberg: Springer) (2006).
[57] Wölfle P, Vollhardt D. Self-consistent theory of Anderson localization: general formalism and applications. *International Journal of Modern Physics B* **24** (2010) 1526–1554.
[58] Saleh BEA, Teich MC. *Fundamentals of photonics* (New York: Wiley) (1991). See Chapter 5, Equation (5.2-14).
[59] Schirmacher W. Thermal conductivity of glassy materials and the boson peak. *Europhys. Letters* **73** (2006) 892.
[60] Marruzzo A, Schirmacher W, Fratalocchi A, Ruocco G. Heterogeneous shear elasticity of glasses: the origin of the boson peak. *Nature Scientific Reports* **3** (2013) 1407.
[61] Schirmacher W, Scopigno T, Ruocco G. Theory of vibrational anomalies in glasses. *Journal of Non-Crystalline Solids* **407** (2015) 133–140.
[62] Abrahams E, Anderson PW, Licciardello DC, Ramakrishnan TV. Scaling theory of localization: Absence of quantum diffusion in two dimensions. *Phys. Rev. Lett.* **42** (1979) 673.
[63] Wegner F. The mobility edge problem: continuous symmetry and a conjecture. *Z. Phys. B* **35** (1979) 207.
[64] Schäfer L, Wegner F. Disordered system with *n* orbitals per site: Lagrange formulation, hyperbolic symmetry, and Goldstone modes. *Zeitschrift für Physik B Condensed Matter* **38** (1980) 113–126.
[65] McKane AJ, Stone M. Localization as an alternative to Goldstone's theorem. *Ann. Phys. (N. Y.)* **131** (1981) 36.
[66] Vollhardt D, Wölfle P. Diagrammatic, self-consistent treatment of the Anderson localization problem in $d \leq 2$ dimensions. *Phys. Rev. B* **22** (1980) 4666–4679.
[67] Vollhardt D, Wölfle P. Scaling equations from a self-consistent theory of Anderson localization. *Phys. Rev. Lett.* **48** (1982) 699–702.
[68] Pritchett TM, Trubatch AD. A differential formulation of diffraction theory for the undergraduate optics course. *Am. J. Phys.* **72** (2004) 1026.
[69] Economou EN, Antoniou PD. Localization and off-diatonal disorder. *Sol. St. Comm.* **21** (1977) 258.
[70] John S, Sompolinsky H, Stephen MJ. Localization in a disordered elastic medium near two dimensions. *Phys. Rev. B* **27** (1983) 5592–5603.
[71] Ganter C, Schirmacher W. *Phys. Rev. B* **82** (2010) 094205.
[72] John S, Stephen MJ. Wave propagation and localization in a long-range correlated random potential. *Phys. Rev. B* **28** (1983) 6358–6368.
[73] Schirmacher W, Schmid B, Tomaras C, Viliani G, Baldi G, Ruocco G, et al. Vibrational excitations in systems with correlated disorder. *physica status solidi (c)* **5** (2008) 862–866.
[74] Abramowitz M, Stegun IA. *Handbook of mathematical functions with formulas, graphs, and mathematical tables*, vol. 55 (US Government printing office) (1964).
[75] Ishimaru A. *Wave propagation and scattering in random media, V* (New York: Academic Press) (1978).
[76] Lee PA, Ramakrishnan T. Disordered electronic systems. *Reviews of Modern Physics* **57** (1985) 287.
[77] Chakravarty S, Schmid A. Weak localization: The quasiclassical theory of electrons in a random potential. *Phys. Reports* **140** (1986) 193.

[78] Schirmacher W, Leonetti M, Ruocco G. Analytical description of the transverse anderson localization of light. *Journal of Optics* **19** (2017) 045602.

[79] Flamini F, Spagnolo N, Sciarrino F. Photonic quantum information processing: a review. *Reports on Progress in Physics* **82** (2018) 016001. doi:10.1088/1361-6633/aad5b2.

[80] Schreiber A, Cassemiro KN, Potoček V, Gábris A, Jex I, Silberhorn C. Decoherence and disorder in quantum walks: From ballistic spread to localization. *Phys. Rev. Lett.* **106** (2011) 180403. doi:10.1103/PhysRevLett.106.180403.

[81] Crespi A, Osellame R, Ramponi R, Giovannetti V, Fazio R, Sansoni L, et al. Anderson localization of entangled photons in an integrated quantum walk. *Nature Photonics* **7** (2013) 322–328.

[82] Giuseppe GD, Martin L, Perez-Leija A, Keil R, Dreisow F, Nolte S, et al. Einstein-podolsky-rosen spatial entanglement in ordered and anderson photonic lattices. *Phys. Rev. Lett.* **110** (2013) 150503. doi:10.1103/physrevlett.110.150503.

[83] Gilead Y, Verbin M, Silberberg Y. Ensemble-averaged quantum correlations between path-entangled photons undergoing anderson localization. *Phys. Rev. Lett.* **115** (2015) 133602. doi:10.1103/PhysRevLett.115.133602.

[84] Aspuru-Guzik A, Walther P. Photonic quantum simulators. *Nature Physics* **8** (2012) 285–291. doi:10.1038/nphys2253.

[85] Harrow AW, Montanaro A. Quantum computational supremacy. *Nature* **549** (2017) 203–209. doi:10.1038/nature23458.

[86] Leonetti M, Karbasi S, Mafi A, DelRe E, Conti C. Secure information transport by transverse localization of light. *Scientific reports* **6** (2016) 29918.

[87] Santagati R, Price AB, Rarity JG, Leonetti M. Localization-based two-photon wave-function information encoding. *Optics express* **27** (2019) 20787–20799.

[88] Lahini Y, Bromberg Y, Christodoulides DN, Silberberg Y. Quantum correlations in two-particle anderson localization. *Physical review letters* **105** (2010) 163905.

[89] Abouraddy AF, Di Giuseppe G, Christodoulides DN, Saleh BEA. Anderson localization and colocalization of spatially entangled photons. *Phys. Rev. A* **86** (2012) 040302. doi:10.1103/PhysRevA.86.040302.

[90] Ambainis A, Bach E, Nayak A, Vishwanath A, Watrous J. One-dimensional quantum walks. *Proceedings of the thirty-third annual ACM symposium on Theory of computing* (ACM) (2001), 37–49. doi:10.1145/380752.380757.

[91] Childs AM. Universal computation by quantum walk. *Phys. Rev. Lett.* **102** (2009) 180501. doi:10.1103/PhysRevLett.102.180501.

[92] Ambainis A. Quantum walks and their algorithmic applications. *International Journal of Quantum Information* **1** (2003) 507–518.

[93] Manouchehri K, Wang J. *Physical Implementation of Quantum Walks* (Berlin, Heidelberg: Springer Berlin Heidelberg) (2014). doi:10.1007/978-3-642-36014-5.

[94] Broome MA, Fedrizzi A, Lanyon BP, Kassal I, Aspuru-Guzik A, White AG. Discrete single-photon quantum walks with tunable decoherence. *Phys. Rev. Lett.* **104** (2010) 153602. doi:10.1103/physrevlett.104.153602.

[95] Geraldi A, Laneve A, Bonavena LD, Sansoni L, Ferraz J, Fratalocchi A, et al. Experimental investigation of superdiffusion via coherent disordered quantum walks. *Phys. Rev. Lett.* **123** (2019) 140501. doi:10.1103/PhysRevLett.123.140501.

[96] Owens JO, Broome MA, Biggerstaff DN, Goggin ME, Fedrizzi A, Linjordet T, et al. Two-photon quantum walks in an elliptical direct-write waveguide array. *New Journal of Physics* **13** (2011)

075003. doi:10.1088/1367-2630/13/7/075003.
[97] Peruzzo A, Lobino M, Matthews JCF, Matsuda N, Politi A, Poulios K, et al. Quantum walks of correlated photons. *Science* **329** (2010) 1500–3. doi:10.1126/science.1193515.
[98] Sansoni L, Sciarrino F, Vallone G, Mataloni P, Crespi A, Ramponi R, et al. Two-particle bosonic-fermionic quantum walk via integrated photonics. *Phys. Rev. Lett.* **108** (2012) 010502. doi:10.1103/physrevlett.108.010502.
[99] Poulios K, Keil R, Fry D, Meinecke JDA, Matthews JCF, Politi A, et al. Quantum walks of correlated photon pairs in two-dimensional waveguide arrays. *Phys. Rev. Lett.* **112** (2014) 143604. doi:10.1103/physrevlett.112.143604.
[100] Preiss PM, Ma R, Tai ME, Lukin A, Rispoli M, Zupancic P, et al. Strongly correlated quantum walks in optical lattices. *Science* **347** (2015) 1229–1233. doi:10.1126/science.1260364.
[101] Caruso F, Crespi A, Ciriolo AG, Sciarrino F, Osellame R. Fast escape of a quantum walker from an integrated photonic maze. *Nat. Commun.* **7** (2016) 11682. doi:10.1038/ncomms11682.
[102] Schreiber A, Cassemiro KN, Potoček V, Gábris A, Mosley PJ, Andersson E, et al. Photons walking the line: A quantum walk with adjustable coin operations. *Phys. Rev. Lett.* **104** (2010) 050502. doi:10.1103/physrevlett.104.050502.
[103] Defienne H, Barbieri M, Walmsley IA, Smith BJ, Gigan S. Two-photon quantum walk in a multimode fiber. *Science Advances* **2** (2016). doi:10.1126/sciadv.1501054.
[104] Cardano F, Massa F, Qassim H, Karimi E, Slussarenko S, Paparo D, et al. Quantum walks and wavepacket dynamics on a lattice with twisted photons. *Sci. Adv.* **1** (2015) e1500087. doi:10.1126/sciadv.1500087.
[105] Cardano F, D'Errico A, Dauphin A, Maffei M, Piccirillo B, de Lisio C, et al. Detection of zak phases and topological invariants in a chiral quantum walk of twisted photons. *Nat. Commun.* **8** (2017) 15516.
[106] Giordani T, Polino E, Emiliani S, Suprano A, Innocenti L, Majury H, et al. Experimental engineering of arbitrary qudit states with discrete-time quantum walks. *Phys. Rev. Lett.* **122** (2019) 020503. doi:10.1103/PhysRevLett.122.020503.
[107] D'Errico A, Cardano F, Maffei M, Dauphin A, Barboza R, Esposito C, et al. Two-dimensional topological quantum walks in the momentum space of structured light. *Optica* **7** (2020) 108–114. doi:10.1364/OPTICA.365028.
[108] Kitagawa T, Broome MA, Fedrizzi A, Rudner MS, Berg E, Kassal I, et al. Observation of topologically protected bound states in photonic quantum walks. *Nat. Commun.* **3** (2012) 882. doi:10.1038/ncomms1872.
[109] Reck M, Zeilinger A, Bernstein HJ, Bertani P. Experimental realization of any discrete unitary operator. *Phys. Rev. Lett.* **73** (1994) 58–61. doi:10.1103/PhysRevLett.73.58.
[110] Clements WR, Humphreys PC, Metcalf BJ, Kolthammer WS, Walmsley IA. Optimal design for universal multiport interferometers. *Optica* **3** (2016) 1460–1465. doi:10.1364/OPTICA.3.001460.
[111] Bromberg Y, Lahini Y, Morandotti R, Silberberg Y. Quantum and classical correlations in waveguide lattices. *Phys. Rev. Lett.* **102** (2009) 253904. doi:10.1103/PhysRevLett.102.253904.
[112] [Dataset] Nielsen MA, Chuang I. Quantum computation and quantum information (2002).
[113] Bennett CH, Brassard G. Quantum cryptography: Public key distribution and coin tossing. *arXiv preprint arXiv:2003.06557* (2020).
[114] Walborn S, Lemelle D, Almeida M, Ribeiro PS. Quantum key distribution with higher-order alphabets using spatially encoded qudits. *Physical review letters* **96** (2006) 090501.
[115] Loudon R. *The quantum theory of light* (OUP Oxford) (2000).

[116] Hong CK, Ou ZY, Mandel L. Measurement of subpicosecond time intervals between two photons by interference. *Phys. Rev. Lett.* **59** (1987) 2044–2046. doi:10.1103/PhysRevLett.59.2044.

[117] Lahini Y, Bromberg Y, Shechtman Y, Szameit A, Christodoulides DN, Morandotti R, et al. Hanbury brown and twiss correlations of anderson localized waves. *Physical Review A* **84** (2011) 041806.

[118] Aaronson S, Arkhipov A. The computational complexity of linear optics. *Proceedings of the Forty-Third Annual ACM Symposium on Theory of Computing* (New York, NY, USA: Association for Computing Machinery) (2011), STOC '11, 333–342. doi:10.1145/1993636.1993682.